Department of Mechanical Engineering
Pennsylvania State University
University Park, PA 16802

Report PSU-ME-R-87/88-0031

Experimental Research on Swept Shock Wave/Boundary Layer Interactions

by Prof. Gary S. Settles

Interim Technical Report for the Period 1 April 1987
to 31 March 1988 on Grant AFOSR-86-0082

submitted to:

Dr. James M. McMichael, Program Manager
US Air Force Office of Scientific Research
Bldg. 410, Bolling AFB, DC 20332-6448

April 1988

PENNSTATE Gas Dynamics Laboratory

UNCLASSIFIED
SECURITY CLASSIFICATION OF THIS PAGE

REPORT DOCUMENTATION PAGE

1a. REPORT SECURITY CLASSIFICATION: Unclassified	1b. RESTRICTIVE MARKINGS
2a. SECURITY CLASSIFICATION AUTHORITY	3. DISTRIBUTION / AVAILABILITY OF REPORT: Approved for Public Release; Distribution Unlimited
2b. DECLASSIFICATION / DOWNGRADING SCHEDULE	
4. PERFORMING ORGANIZATION REPORT NUMBER(S): PSU-ME-R-87/88-0031	5. MONITORING ORGANIZATION REPORT NUMBER(S): AFOSR-TR- 88-0687
6a. NAME OF PERFORMING ORGANIZATION: Dept. of Mechanical Engrg., Penn State University	6b. OFFICE SYMBOL (If applicable):
	7a. NAME OF MONITORING ORGANIZATION: Air Force Office of Scientific Research
6c. ADDRESS (City, State, and ZIP Code): University Park, PA 16802	7b. ADDRESS (City, State, and ZIP Code): Building 410, Bolling AFB, Washington, DC 20332
8a. NAME OF FUNDING / SPONSORING ORGANIZATION: Air Force Office of Sci. Res.	8b. OFFICE SYMBOL (If applicable): AFOSR/NA
	9. PROCUREMENT INSTRUMENT IDENTIFICATION NUMBER: AFOSR-86-0082
8c. ADDRESS (City, State, and ZIP Code): Building 410, Bolling AFB, Washington, DC 20332	10. SOURCE OF FUNDING NUMBERS: PROGRAM ELEMENT NO. 61102F; PROJECT NO. 2307; TASK NO. A1; WORK UNIT ACCESSION NO.

11. TITLE (Include Security Classification)
Experimental Research on Swept Shock Wave/Boundary Layer Interactions

12. PERSONAL AUTHOR(S)
Gary S. Settles

13a. TYPE OF REPORT	13b. TIME COVERED	14. DATE OF REPORT (Year, Month, Day)	15. PAGE COUNT
Annual TR	FROM 87/4/1 TO 88/3/31	88/4/28	56

16. SUPPLEMENTARY NOTATION

17. COSATI CODES		
FIELD	GROUP	SUB-GROUP

18. SUBJECT TERMS (Continue on reverse if necessary and identify by block number)
High-Speed Flows; Viscous-Inviscid Interactions; Shock-Boundary Layer Interactions; Supersonic Flow, Experiments; Flow Visualization; Fluid Dynamics; Flow Separation

19. ABSTRACT (Continue on reverse if necessary and identify by block number)

The second year of an experimental study of swept shock wave interactions with turbulent boundary layers is reported. This work relied entirely on non-intrusive, laser-based optical flow diagnostics. Experiments were carried out to define the flowfield structure of fin-generated interactions over a Mach number range from 2.5 to 3.5 using the laser light-screen flow visualization technique. Further experiments resulted in accurate skin friction measurements in fin-generated swept interactions by way of the Laser Interferometer Skin Friction Meter. Finally, techniques were perfected for the assessment of flowfield fluctuation levels using pulsed-laser holographic interferometry. The results of this research have given new insight into the fin-interaction flowfield structure, which involves a supersonic jet produced by shock wave refraction and impinging on the test surface. High skin friction levels were measured in the vicinity of this jet impingement, which compare well with computational predictions carried out by others. Finally, the observed jet impingement structure is shown to be similar to that of leading-edge shock wave impingement on high-speed flight vehicles.

20. DISTRIBUTION / AVAILABILITY OF ABSTRACT: ☒ UNCLASSIFIED/UNLIMITED ☐ SAME AS RPT. ☐ DTIC USERS	21. ABSTRACT SECURITY CLASSIFICATION: UNCLASSIFIED
22a. NAME OF RESPONSIBLE INDIVIDUAL: James M McMichael	22b. TELEPHONE (Include Area Code): 202-767-4936 / 22c. OFFICE SYMBOL: AFOSR/NA

DD FORM 1473, 84 MAR — 83 APR edition may be used until exhausted. All other editions are obsolete.

SECURITY CLASSIFICATION OF THIS PAGE
UNCLASSIFIED

Table of Contents

I. Summary

The second year of an experimental study of swept shock wave interactions with turbulent boundary layers is reported. This work relied entirely on non-intrusive, laser-based optical flow diagnostics. Experiments were carried out to define the flowfield structure of fin-generated interactions over a Mach number range from 2.5 to 3.5 using the laser light-screen flow visualization technique. Further experiments resulted in accurate skin friction measurements in fin-generated swept interactions by way of the Laser Interferometer Skin Friction Meter. Finally, techniques were perfected for the assessment of flowfield fluctuation levels using pulsed-laser holographic interferometry. The results of this research have given new insight into the fin-interaction flowfield structure, which involves a supersonic jet produced by shock wave refraction and impinging on the test surface. High skin friction levels were measured in the vicinity of this jet impingement, which compare well with computational predictions carried out by others. Finally, the observed jet impingement structure is shown to be similar to that of leading-edge shock wave impingement, which is known to produce serious pressure and heating loads on aerodynamic surfaces of high-speed flight vehicles.

II. Research Objectives

The research objectives for the second year of AFOSR Grant 86-0082, as given in the Statement of Work of our proposal dated December 1, 1986, were as follows:

1) Explore the flowfield structure of swept interactions due to sharp fins at Mach 3 and variable α (fin angle of attack) by way of optical diagnostics.

2) For the same flow conditions, apply pulsed-laser holographic interferometry to assess flowfield fluctuation levels.

3) Obtain 3-D skin friction measurements in these flows using the Laser Interferometer Skin Friction Meter.

Progress toward the achievement of these research objectives is discussed in detail in the following section.

III. Status of the Research - Accomplishments and Progress

1) Optical Flowfield Structure Results

The flowfield structure of shock wave/turbulent boundary layer interactions at Mach numbers 2.5, 3, and 3.5 has been investigated as proposed during the second year of the subject Grant. Sharp, unswept-leading-edge fins were used to generate swept planar shock

waves which interacted with the two-dimensional, equilibrium turbulent boundary layer on an adiabatic flat plate. The shock wave strength was varied by adjustable fin angles of attack up to a maximum of 18 degrees. The flowfield structure was observed by the laser light-screen technique (Ref. 1), in which the beam from a 5-watt Argon-ion laser was expanded into a thin sheet and passed through the flow normal to the swept shock wave. Moisture was added to the airstream of the Penn State Supersonic Wind Tunnel, so that the cross-section of the airstream became visible due to Mie scattering of the laser sheet. The results were then photographed, yielding quantitative structural information over the parameter ranges stated. Since laser light-screen results are inherently of low contrast, digital image processing has been used for contrast enhancement.

Some previously-known features of the flowfield structure, such as the separation shock, "lambda-foot," and triple point, were clearly revealed. The evolution of these features with increasing shock strength (ie increasing Mach number or fin angle) has been quantified. Weak interactions appear nearly featureless, but distinct structural features appear and evolve as the shock strength increases. From these results we have ascertained the following:

* clear images of detailed flowfield structures can be obtained
* these structures evolve with increasing shock strength
* supersonic jet impingement is seen in strong interactions
* computations and surveys have not revealed these features

An important discovery of this work is the flowfield structure *downstream* of the triple-point in strongly separated interactions, which has not been observed previously. An example of such a light-screen image, with contrast enhanced by digital image processing, is shown in Fig. 1. (Complete details of this and related flow images obtained in this research are given in Appendix A, which conveys the draft version of a paper to be presented at the First National Fluid Dynamics Congress, Cincinnati OH, July 1988.) A supersonic jet is seen in Fig. 1 to emanate from the "lambda-shock" structure, curve downward, and impinge on the test surface, leading to hign local pressure and heating. This phenomemon appears closely related to Edney-type (Ref. 2) leading-edge shock interference. Earlier flowfield models, such as that of Zheltovodov (Ref. 3) do not show the flowfield structure as it is here revealed to exist.

While both flowfield surveys and Navier-Stokes simulations have been carried out previously for interactions similar to that of Fig. 1, neither has had the resolution to reveal the critical downstream structure. For example, Figs. 2 and 3 show the flowfield structures of strong fin interactions surveyed by Kimmel (Ref. 4) and computed by Knight (Ref. 5). In the former case, one is forced to conclude that contours interpolated from flowfield surveys are simply not well adapted to revealing structural details (at least, not at the resolution shown). For the latter, the coarse mesh employed in the flowfield to economize on computer storage causes structural features, even including the main shock wave, to be smeared into indistinction. Discussions with D. Knight and C. Horstman of the AFOSR 3-D Shock Wave/Turbulent Boundary Layer Interaction Working Group reveal that there is insufficient memory in the available supercomputers to allow resolving the flowfield to the required level.

2) Laser Interferometer Skin Friction Results

Measurements by Laser Interferometer Skin Friction Meter (LISF) of the Mach 3, α = 10° and 16° fin interactions have been successfully carried out in the Penn State Supersonic Wind Tunnel. In order to carry out these experiments it has been necessary to reconfigure our LISF instrument to look directly down on the flat plate test surface from above. Also, a replacement test section ceiling was designed and constructed to contain the plexiglass window needed for optical observation from above. Having made the necessary modifications to the LISF instrument and tunnel ceiling, we ran kerosene-lampblack surface flow visualization traces of the Mach 3, α = 10° and 16° fin interactions to recheck the flow quality, which was found to be quite good.

Since LISF measurements are pointwise and time-consuming, some consideration was given to the proper location of the measuring positions on the flat plate. First of all, since *no skin friction data of established accuracy exist for any swept interaction*, we wished to produce data which will serve as a "benchmark." It thus seems reasonable to acquire data in the region from the undisturbed boundary layer to the fin in the zone of quasiconical flow symmetry, ie, outside the interaction inception zone. (Measurements inside the inception zone provide less general information, thus are assigned a lower priority.) Secondly, we are thus making use of the inherent symmetry of the interaction, which calls for a spherical polar system of coordinates. For surface measurements, such coordinates form concentric circular arcs centered about the virtual concial origin of the flow (see, eg, Ref. 6 for a detailed discussion of optimum interaction coordinate systems). However, it was our intention to measure interactions of different α in this way, and the virtual origin changes with α. Since the virtual origin is not far displaced from the fin leading edge, we have chosen the latter as the origin of coordinates for simplicity. Note that some investigators still remain confused about the optimum coordinate frame of swept interactions. We believe strongly that *the measurement of data along lines parallel to the freestream in swept interactions, as was done in early studies, is confusing and inappropriate in the light of current understanding.*

The chosen datum radius for detailed skin friction data in the Mach 3, α = 10° fin interaction was 4.5 inches from the fin leading edge. This was chosen to be well downstream of the inception zone according to the established scaling law for that zone (Ref. 1):

$$(L_i/\delta_0)Re\delta_0{}^a = \kappa_1 \cdot \tan\lambda_s \qquad (1)$$

where $a \simeq 1/3$ at Mach 3, $\kappa_1 \simeq 1133$, and λ_s is the sweepback angle of the fin shock. For our current tests at Re = 5.9×10^7/meter and δ_0 = 4.2 mm, Eqn. 1 yeilds an inception length L_i of about 2 inches from the fin leading edge. By making use of the quasiconical symmetry of the interaction, it is possible to plot the LISF data vs. angle β from the freestream direction. The results will thus automatically be in dimensionless coordinates (as, indeed, all conical flows must be).

The LISF skin friction data for the Mach 3, α = 10° and 16° interactions are shown in these coordinates in Figs. 4 and 5. Also shown are the Navier-Stokes compuational predictions of Horstman (private communication) and Knight (Ref. 7). Figs. 4 and 5 are very revealing and bear some discussion.

First of all, the reason to obtain LISF data is that *there is no other known technique which will measure skin friction with known accuracy in a shock/boundary layer interaction.* The Preston-tube method is much simpler to use than LISF, but does not actually measure skin friction. Instead, it measures pitot pressure at the wall and *infers* skin friction through a

calibration which cannot be trusted in a strongly-interacting flow. Further, reliable skin friction data are sorely needed to test the predictive capabilities of current Navier-Stokes solvers. Here, representative state-of-the-art computations are tested against *reliable* data with an established accuracy of ± 5%.

In brief, it appears that both computations have done well. Both Knight's and Horstman's CFD results are in good agreement with the LISF skin friction measurements at both fin angles of attack. Upon close inspection, the LISF data show a slight initial rise in c_f at the beginning of the interaction, which is displaced downstream in Horstman's computed prediction and missing altogether from Knight's. Nonetheless, the comparison is well summarized by a quote from Prof. Knight upon seeing these results: "I'm surprised that the computations did this well."

Though the LISF technique measures skin friction, in principle, with equal facility in or out of an interacting flow, we have experienced the following problem. As shown in Figs. 4 and 5, c_f rises by as much as a factor of 4 in the interaction, above its undisturbed flat-plate level. At very high wall shear levels the problem of surface-wave instabilities on the oil film limits the number of obtainable LISF fringes, and thus the accuracy of the result. Monson (Ref. 8) reckoned the maximum wall shear level measureable by LISF to be about 150 N/m^2. By way of technique refinements and improved data analysis we have reached perhaps four times this value, though at the cost of a somewhat larger error band at peak c_f levels. A complete discussion of this issue, as well as of the LISF instrument and the experiments described above, is included in AIAA Paper 88-0497 which forms Appendix B of this Report.

In summary, we have learned the following thus far from the LISF experiments:

* the LISF technique works in swept interactions
* a surface-wave limitation is present but not overriding
* initial results compare well with CFD predictions
* more comparisons for stronger interactions are needed

Finally, the high peak shear levels revealed in Figs. 4 and 5 are connected, we believe with the flowfield structure results described earlier. Peak c_f is seen to occur in the vicinity of the supersonic jet impingement noted in the previous section. Thus much of the skin friction behavior within these swept interactions may be thought of as a *decay* from peak levels beneath the jet impingement, forward to the upstream influence line. The fact that the computations predict this well seems to indicate that the important flow physics is present in the computations, though they do not adequate resolve such flow phenomena as the jet impingement.

Finally, the Reynolds-averaged Navier-Stokes results of Horstman and Knight do not address flowfield unsteadiness, which seems almost certain to be present in the peak c_f region. For that matter, no experimental data on unsteadiness are available there either. This is definitely an issue for future research.

3) Pulsed-Laser Holographic Interferometry Results

Our efforts to apply pulsed-laser holographic interferometry to swept interactions, as indicated in the earlier statement of research objectives, are still incomplete at the time of this writing. We have, however, completed the proof-of-concept optical bench tests which are prerequisite to applying this flow diagnostic in actual wind tunnel experiments. A wind tunnel entry is scheduled for May, 1988, to obtain holographic interferograms in fin-generated shock/boundary layer interactions.

Pulsed-laser holographic interferometry is both a valuable and a difficult flow diagnostic. Its value lies in its ability to obtain true 3-D flowfield images, to generate a series of holographic interferograms revealing different ranges of flowfield fluctuations, to image the flow through poor optical components or even against opaque backgrounds, and to provide quantitative density measurements. Some of the difficulties include: complex laser operation, limited laser reliability and repeatability, extended user training, and limited optical access to 3-D flows in conventional wind tunnels.

We have made significant progress in most of these areas, with a few difficulties left to overcome. Two members of our research team are now proficient in the operation of the Gas Dynamics Lab's 300 mJ double-pulse ruby laser, and others are learning the technique. Beyond this, we have also developed and demonstrated the following capabilities:

* High-quality holographic interferogram production
* Both 2-D and 3-D interferometric imaging of interacting flows
* Flow fluctuation analysis by variable-pulse-separation holography
* Flow imaging through plexiglass and against opaque backgrounds

Two examples of this capability are shown here in Figs. 6 and 7. Both are photographs obtained recently in our Laboratory, depicting reconstructions of holographic interferograms of an axisymmetric supersonic free jet (Fig. 6) and a converging nozzle with internal shock/boundary layer interaction and separation (Fig. 7). In both cases, small-scale, benchtop flows were established for technique development and evaluation (both flow phenomena appear at near full scale in these Figures). These image-plane holograms are reconstructed in white light - one of several possible methods - which results in superimposed rainbow diffraction colors on the interferograms.

In Fig. 6, an overexpanded free jet with Mach number about 2.5 exists from the axisymmetric nozzle appearing in the upper left of the photograph. This double-pulse holographic interferogram was exposed once with no flow, then again with flow on. The entire range of mean and fluctuating densities in the jet is thus revealed. Other interferograms in this series (not shown here) were taken with progressively shorter intervals between laser pulses while the flow was on. These reveal the location and magnitude of flow fluctuations within a given frequency passband. For example, a pulse separation of 500 μs results in a holographic interferogram revealing only those flow components with frequencies greater than $1/(500\times10^{-6})$ = 2 kHz. As this frequency high-pass cutoff is raised, first the shock waves and eventually the turbulent structures disappear from the interferogram. For the jet in Fig. 6, pulse separations less than about 15 μs reveal no remaining fluctuations (above $\simeq$ 67 kHz).

Fig. 7 is a photo of the white-light interferogram reconstruction of a "2-D" supersonic nozzle flow. Shock-induced separation and an irregular shock crossing are apparent just before the nozzle exit at the far right in the Figure. The main significance of this image is that it was taken through two ordinary plexiglass sidewalls. Internal strains in the plexiglass usually prevent other optical flow imaging methods (*eg* schlieren and shadowgraph) from functioning. We intend to put this capability to use by using extended plexiglass sidewall and diffuser windows in the Penn State Supersonic Wind Tunnel in order to obtain the highly-oblique viewing angles necessary to image swept shock/boundary layer interactions. These windows are already fabricated and are awaiting use in an upcoming tunnel entry.

The remaining problems to be solved in implementing holographic interferometry as described in the Research Objectives section mainly concern the pulsed-ruby laser itself. Although it is essentially new, it suffers occasional operational lapses which have delayed its use in actual wind tunnel tests until now. We are currently negotiating with the instrument's manufacturer (Apollo Lasers, Inc.) to resolve these problems.

Meanwhile, as just discussed, we have developed an arsenal of holographic interferometry techniques and capabilities during the grant year reported here that will allow us to accomplish this part of the stated research objectives. We regard this work as a top priority item, insofar as time-resolved data in swept interactions are extremely sparse, and *none* of the available results address the fluctuations of the interaction flowfield at all. Thus the time-resolved nature of these flow is almost completely unknown. It is, further, a key issue in our fundamental understanding of swept interaction behavior, as well as in the validation of current CFD predictions which are time-averaged. Experimental results directly addressing this issue are anticipated during the first quarter of the 1988-89 AFOSR grant year.

4) Other Significant Accomplishments

In addition to the research described above, carried out in direct fulfillment of the Statement of Work for the second year of the subject Grant, additional related work has been done during the second-year reporting period. In particular, we have put into operation the research equipment obtained under AFOSR Grant 84-184, a DoD-URIP Grant now expired which was specifically for equipment in support of our research on shock/boundary-layer and related high-speed viscous-inviscid interactions.

An example is documented in Appendix C, which contains AIAA Paper 88-2062 on the subject of microprocessor control of high-speed wind tunnel stagnation pressure. The microprocessor controller and transducers obtained under AFOSR Grant 84-184 were put into operation to provide automatic stagnation pressure control of the Penn State Supersonic Wind Tunnel Facility. The accompanying analysis and experimental verification have also resulted in a Masters Degree for one member of our research group.

Many other examples could be cited of equipment obtained earlier under AFOSR Grant 84-184 which is now in use and contributing to the currently-reported research. These items include, in particular, the test section assembly, Argon-ion laser, Chronolite-8 and Hycam II high-speed cameras, and data acquisition system obtained under the DoD-URIP program. These are cited here because of their crucial impact on our ability to have obtained the successful results described in this report.

IV. Plans for Third-Year Effort

The third year of AFOSR Grant 86-0082 is now under way. Our goals for this effort center around the use of our established capability in non-intrusive, laser-based optical flow diagnostics to attempt to resolve some of the key questions concerning the swept shock/boundary layer interaction phenomenon. Early in this year, 3-D pulsed-laser holographic interferometry, as described above, will be brought to bear on the problem of swept interaction unsteadiness and structure. Our further goals are listed below, from the Statement of Work of our proposal dated October, 1987:

1) Further investigate the detailed structures of swept fin-generated interactions, including both weak and strong cases, using pulsed-laser holography.

2) Apply laser light-screen diagnostics to examine the growth of weak and strong interactions with distance downstream of the interaction apex.

3) Widen the current database of LISF skin friction measurements in these flows to include Mach numbers higher than 3.

4) Explore the improvement of LISF instrument performance at high wall shear levels.

V. Publications

1) Settles, G. S., Metwally, O. M., Hsu, J., and McIntyre, S. S., "Visualization of High-Speed Flows at the Penn State Gas Dynamics Laboratory," Invited paper to be presented at the 1988 International Conference on Lasers and Electro-Optics, Santa Clara, Oct. 30, 1988. (*in preparation.*)

2) Fung, Y-T, Settles, G. S., and Ray, A., "Microprocessor Control of High-Speed Wind Tunnel Stagnation Pressure," to be presented at the AIAA Aerodynamic Testing Conference, San Diego, CA, May 18-20, 1988.

3) Lu, F. K., and Settles, G. S., "Structure of Fin-Shock/Boundary Layer Interactions by Laser Light-Screen Visualization," to be presented at the 1st National Fluid Dynamics Congress, Cincinnati, July 1988.

4) Kim, K-S, and Settles, G. S., "Skin Friction Measurements by Laser Interferometry in Swept Shock Wave/Turbulent Boundary-Layer Interactions," AIAA Paper 88-0497, presented at the AIAA 26th Aerospace Sciences Conference, Reno, NV, January 11-14, 1988. (*Submitted for publication to AIAA Journal and now undergoing review.)*

5) Settles, G. S., "Aerospace and Wind Tunnel Testing," Chapter IV-4 of *Handbook of Flow Visualization*, ed. W.-J. Yang, Hemisphere Press. (*To be published in 1988.)*

6) Kim, K.-S., and Settles, G. S., "Skin Friction Measurements by Laser Interferometry," Ch. 3 of an AGARDograph entitled *A Survey of Measurements and Measuring Techniques in Rapidly Distorted Compressible Turbulent Boundary Layers*, eds. H. H. Fernholz, A. J. Smits, and J.-P. Dussauge, (*To be published in 1988.)*

7) Lu, F. K., Settles, G. S., and Horstman, C. C., "Mach Number Effects on Conical Surface Features of Swept Shock Boundary-Layer Interactions," AIAA Paper 87-1365, June 1987, (*Accepted for publication in AIAA Journal.*)

VI. Personnel

Principal Investigator

Prof. Gary S. Settles

Graduate Research Assistants

Joseph C. Hsu (Ph.D. candidate supported by the subject Grant)

Kwang-Soo Kim (Ph.D. candidate supported by the subject Grant. Dissertation entitled "The Laser Interferometer Skin Friction Meter for Compressible Flows," in preparation. Graduation expected during 1988.)

Frank K. Lu (Ph.D. candidate supported in part by the subject Grant and in part by NASA-Ames Interchange Agreement NCA2-192. Thesis title: "Fin-Generated Shock Wave/-Boundary Layer Interactions." Degree will be granted on May 14, 1988.)

VII. Interactions

1) Spoken Papers at Meetings, Conferences, and Seminars

1) Kim, K-S, and Settles, G. S., "Skin Friction Measurements by Laser Interferometry in Swept Shock Wave/Turbulent Boundary-Layer Interactions," AIAA Paper 88-0497, presented at the AIAA 26th Aerospace Sciences Conference, Reno, NV, January 11-14, 1988.

2) Settles, G. S., "Comments on Useful vs. Unproductive Code Validation Exercises," presented at the NASA CFD Validation Workshop, Moffett Field, CA, July 14-16, 1987.

3) Settles, G. S., "Current and Planned Shock Wave/Turbulent Boundary Layer Research at Penn State," presented at the First Annual 3-D Shock/Boundary Layer Interaction Working Group Meeting, University Park, PA, July 27-28, 1987.

4) Lu, F. K., Settles, G. S., and Horstman, C. C., "Mach Number Effects on Conical Surface Features of Swept Shock Boundary-Layer Interactions," AIAA Paper 87-1365, presented at the AIAA 19th Fluid and Plasma Dynamics Conference, Honolulu, HI, June 1987.

2) Consultative and Advisory Functions

• Dr. C. C. Horstman of NASA-Ames Research Center visited our group on April 6-7, 1987. Detailed discussions of shock/boundary layer interaction problems were held.

• Dr. A. G. Havener of SUNY-Binghamton University visited our group on April 9, 1987. His expert advice on holographic interferometry issues was sought.

• PI visited Princeton University May 7, 1987, to participate as External Reader in the Ph.D. Defense of Roger L. Kimmel, a student of Prof. Bogdonoff whose work concerned swept interactions.

• PI and F. K. Lu attended AIAA 19th Fluid and Plasma Dynamics Conference, Honolulu, HI, June 1987. AFOSR-supported work was presented (see above). Many discussions were held with colleagues involved in swept interaction research and related issues.

• PI and several group members attended AFOSR/ONR Contractors Meeting at Penn State the week of June 21, 1987. Discussions were held with Dr. Tishkoff of AFOSR and many others.

• PI visited US Naval Weapons Center, China Lake, CA, on July 13, 1987 to assist Drs. E. Gutmark and K. Schadow with optical flow diagnostic experiments.

• PI attended NASA CFD Validation Workshop at Ames Research Center July 14-16, 1987, and presented AFOSR-supported research to participants (see above).

• PI participated in transonic wing tests at NASA-Ames Research Center, July 14, 1987, and instructed personnel there on the proper use of surface flow visualization method.

• PI met with R. S. Boray of AFWAL/POPT July 16, 1987 and discussed LISF skin friction instrument. Copy of technical paper was later sent to Boray.

• PI met with Lockheed Corp. personnel T. Harsha, L. Long, and P. Bevilacqua on July 17, 1987 to discussed cooperation on hypersonic swept interaction experiments.

• PI discussed with F. Staub of GE Corp. (Schenectady, NY) possible PSU facility use for govt.-sponsored GE testing program, July 23, 1987.

• PI hosted the First Annual 3-D Shock/Boundary Layer Interaction Working Group Meeting, University Park, PA, July 27-28, 1987. Composed primarily of AFOSR-supported investigators, this Group produced a document outlining future research needs. Dr. J. D. Wilson of AFOSR was present along with 8 others.

• Dr. E. Gutmark of the US Naval Weapons Center, China Lake, CA, visited our group on Aug. 12, 1987, presented a seminar, and participated in detailed research discussions.

• PI discussed with E. Kawecki of Pratt & Whitney Corp. possible consulting arrangement for advice to P&W NASP program on shock/boundary layer interactions, Sept. 25, 1987.

• Dr. M. Reichman of ONR visited our group on Sept. 30, 1987. He was given a tour of our facilities and discussions of high-speed propulsion research were held.

• Mr. George Donahue of the RAND Corp. visited Penn State on Sept. 30, 1987. PI discussed with him issues concerning NASP aerodynamics and propulsion.

• Dr. C. C. Horstman of NASA-Ames Research Center visited our group on October 26-27, 1987. Detailed discussions of shock/boundary layer interaction problems were held.

• Dr. S. Lekoudis of ONR visited Penn State on October 27, 1987 regarding proposed supersonic mixing research under joint ONR/AFOSR sponsorship.

• Dr. T. Doligalski of the US Army ARO visited our group on October 28, 1987. Discussions were held of mutual research interests and a facility tour was given.

• Dr. A. Gross of NASA-Ames visited Penn State on December 3, 1987, and was given a tour of our facilities and a presentation on our research program.

• PI was quoted in NY Times article January 5, 1988, concerning swept interaction research and high-speed test facilities.

• PI and K-S Kim attended AIAA 26th Aerospace Sciences Meeting, Reno, NV, Jan. 11-14, 1988. Presented AFOSR-supported work (see above). Attended sessions on shock/boundary layer interactions and related topics. Held discussions with co-workers in this research area including S. M. Bogdonoff, C. C. Horstman, D. D. Knight, D. S. Dolling, & G. R. Inger at 2nd Meeting of the 3-D Shock/Boundary Layer Interaction Working Group.

• PI met with Dr. J. McMichael of AFOSR to discuss current research program and plans, Jan. 12, 1988 in Reno, NV.

• PI received invitation to attend Soviet Conference on Simulation Problems and Wind Tunnels from Dr. A. A. Zheltovodov (ITAS Novosibirsk) on Jan. 19, 1988 (Declined due to conflict with 1st Natl. Fluid Dynamics Congress.)

• PI discussed heat transfer instrumentation with R. Neumann of AFWAL on Feb. 24, 1988.

• PI discussed possible visiting scientist arrangement at AFWAL with J. Shang and K. Stetson of AFWAL on March 8, 1988 (at their request; negotiations in progress).

• PI rendered advice to Rocketdyne Corp. personnel J. Skipper, J. Blauer, and L. Rubin on holographic interferometry for NASP testing program, March 10, 22, and 24, 1988.

VIII. References

1) Settles, G. S., "Modern Developments in Flow Visualization," Invited Survey Paper No. AIAA 84-1599, and *AIAA Journal*, Vol. 24, No. 8, August, 1986, pp. 1313-1323.

2) Edney, B., "Anomalous Heat Transfer and Pressure Distributions on Blunt Bodies at Hypersonic Speeds in the Presence of an Impinging Shock," FFA Report 115, 1968.

3) Zheltovodov, A. A., "Properties of Two- and Three-Dimensional Separation Flows at Supersonic Velocities, *Izvestiya Akademii Nauk SSSR, Mekhanika Zhidkosti i Gaza*, Vol. 14, May-June 1979, pp. 42-50.

4) Private communication, R. L. Kimmel, April 28, 1986

5) Gaitonde, D., and Knight, D. D., "The Effect of Bleed on the Flowfield Structure of the 3-D Shock Wave - Boundary Layer Interaction Generated by a Sharp Fin," paper submitted for AIAA presentation.

6) Settles, G. S., and Dolling, D. S., "Swept Shock Wave-Boundary Layer Interactions," in "Tactical Missile Aerodynamics," eds. M. J. Hemsch and J. N. Nielsen, Vol. 104 of *AIAA Progress in Astronautics and Aeronautics Series*, September, 1986, pp. 297-379.

7) Knight, D. D., Private communication, October 10, 1987.

8) Monson, D. J., Driver, D. M., and Szodruch, J., "Application of a Laser Interferometer Skin Friction Meter in Complex Flows," *ICIASF Proceedings*, 1981, pp. 232-243.

IX. Figures

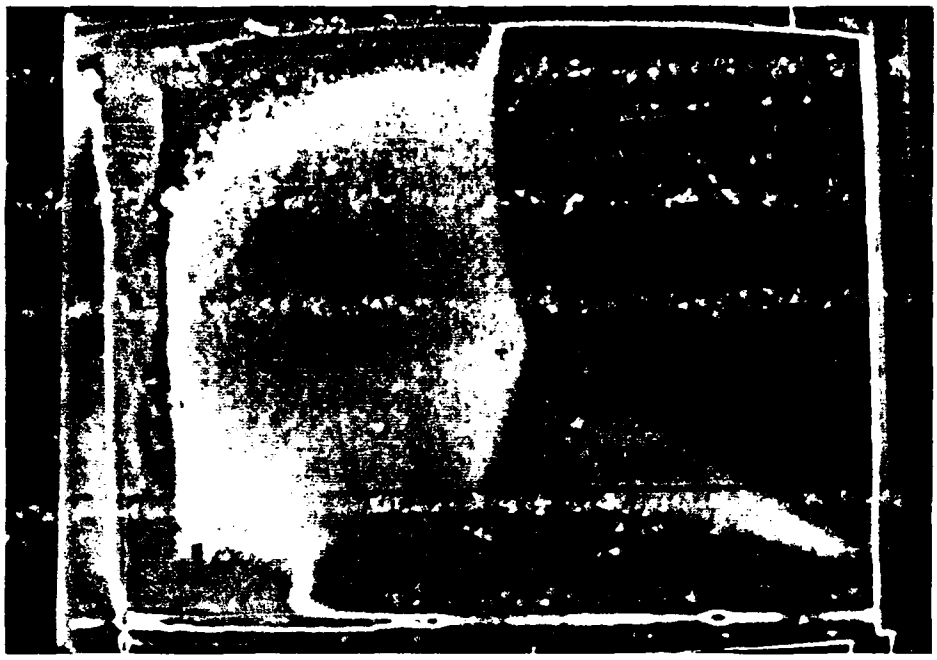

Fig. 1 - Laser Light-Screen Image of Flowfield Structure, Fin Interaction, Mach 3.5, α = 15°

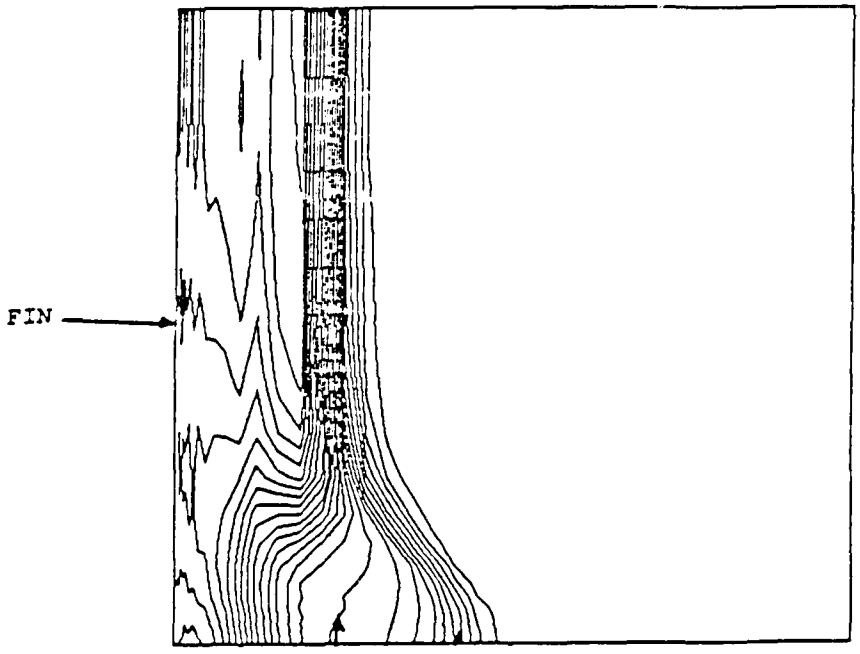

Fig. 2 - CFD Static Pressure Contours of Mach 3, α = 20° Interaction (Knight, Ref. 5)

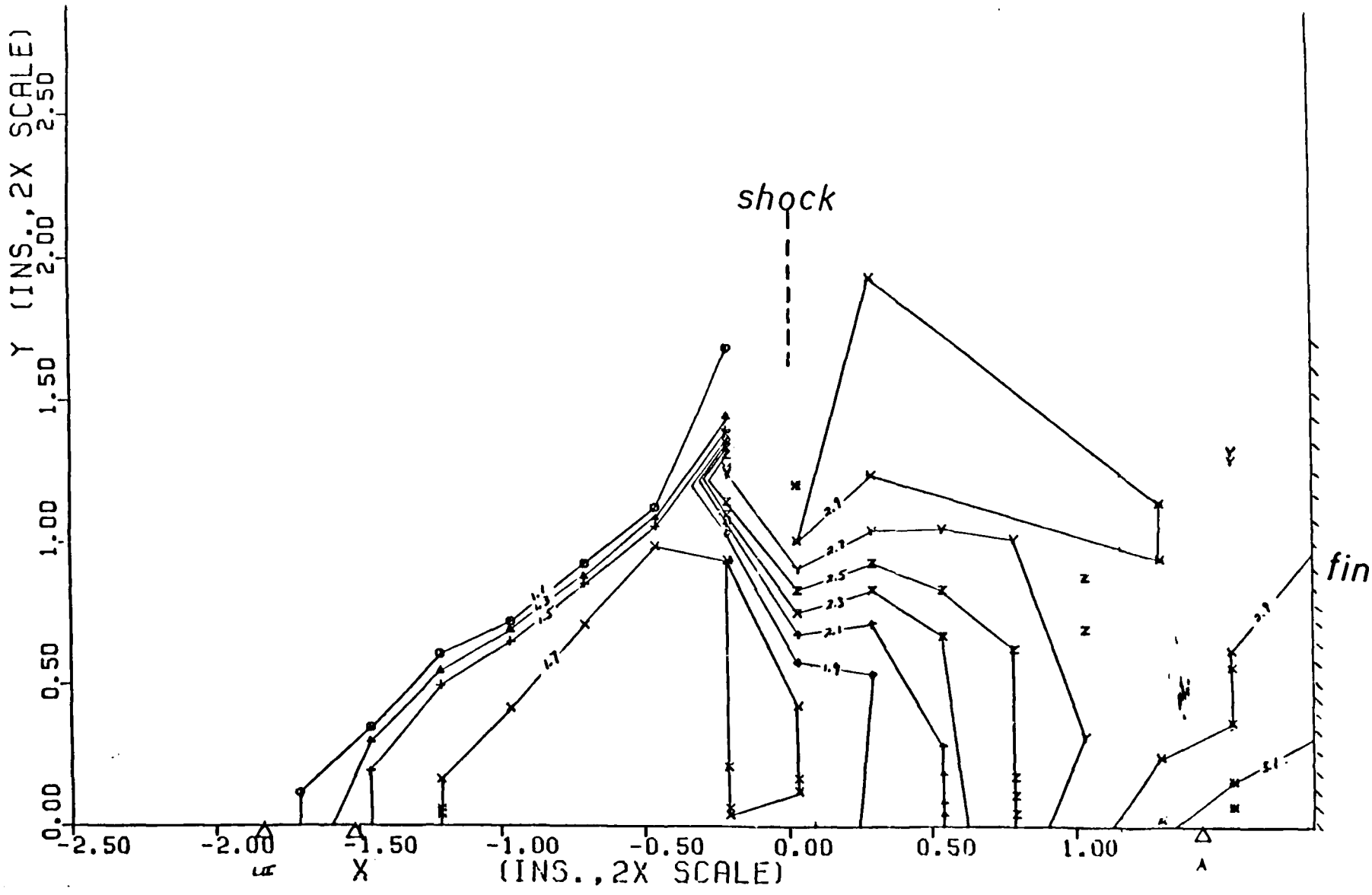

Fig. 3 - Static Pressure Contours of the $M_\infty = 3$, $\alpha = 20°$ Fin Interaction, from Flowfield Surveys by Kimmel (Ref. 4).

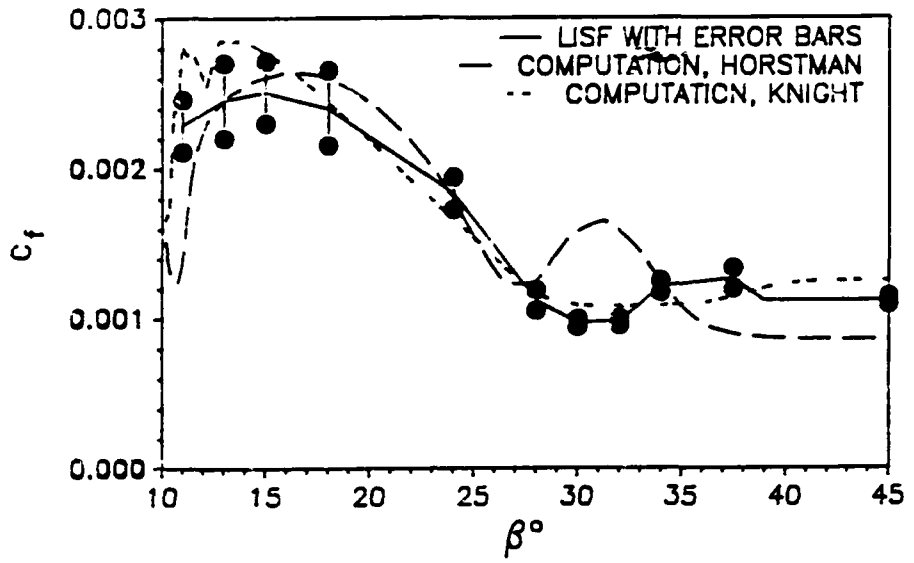

Fig. 4 - Comparison of Fin-Interaction LISF Data with Computations, Mach 3, α = 10°.

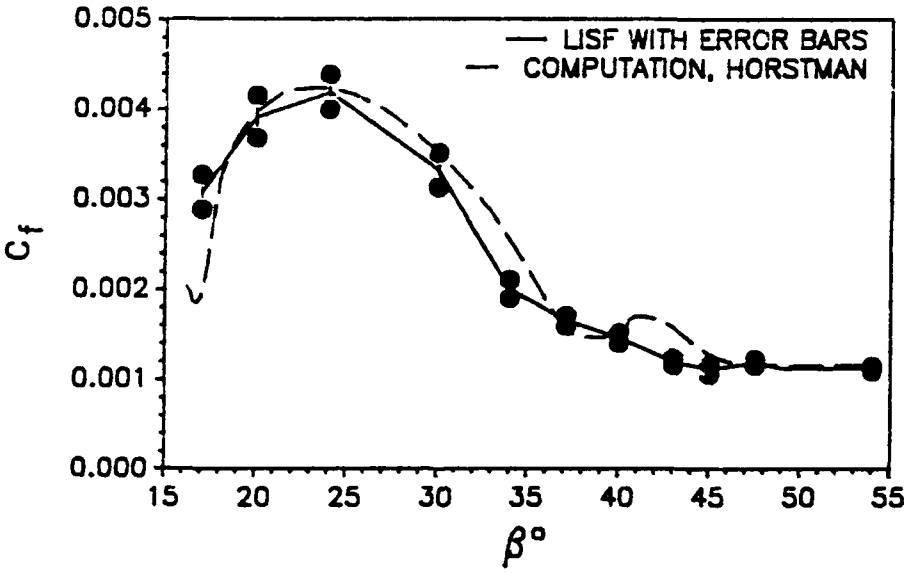

Fig. 5 - Comparison of Fin-Interaction LISF Data with Computations, Mach 3, α = 16°.

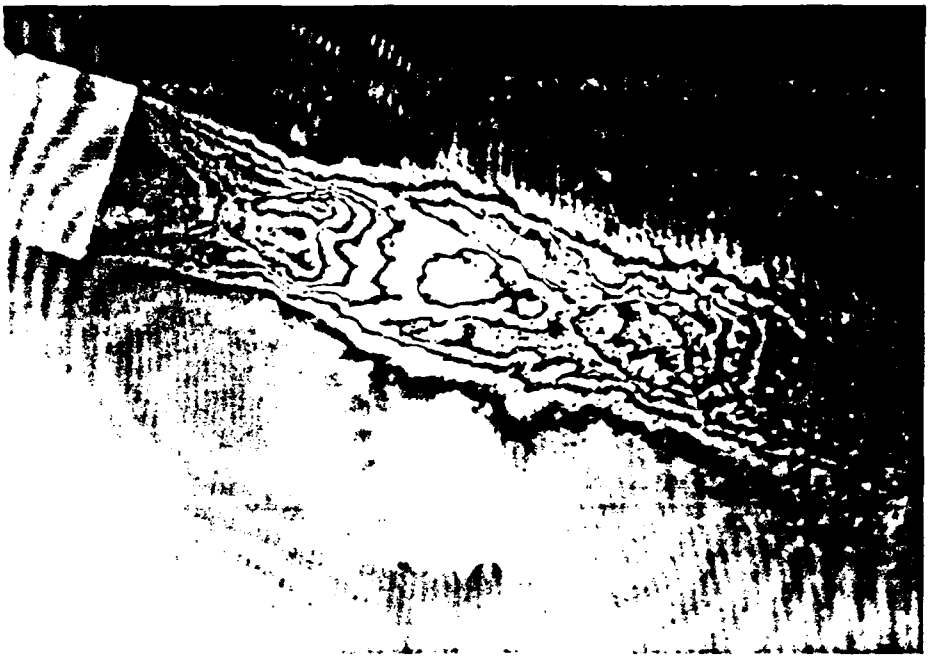

Fig. 6 - Holographic Interferogram of Overexpanded Axisymmetric Supersonic Jet.

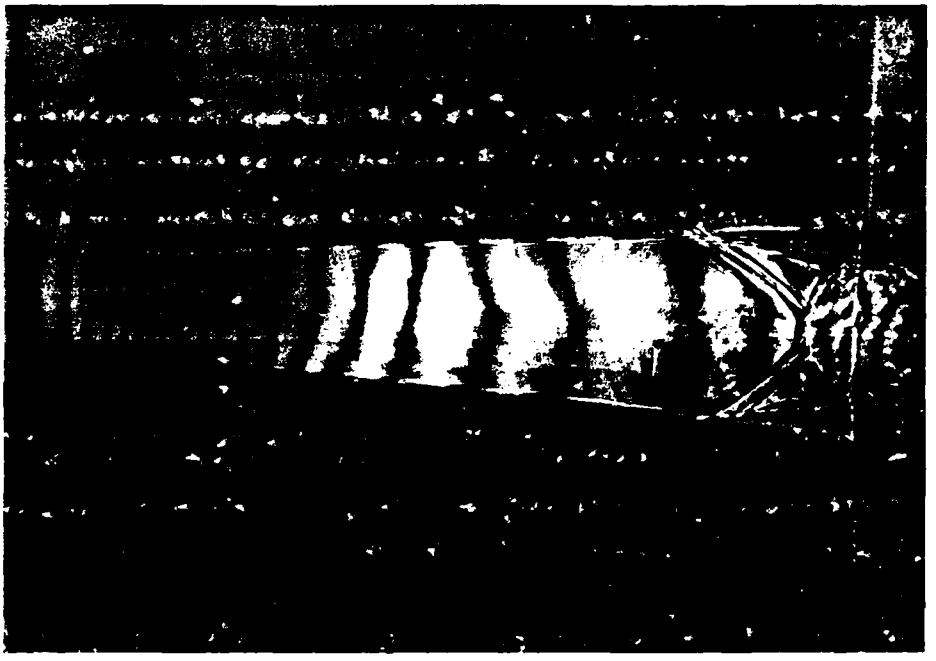

Fig. 7 - Holographic Interferogram of 2-D Nozzle Flow with Shock-Induced Separation.

X. Appendix A

AIAA-88-

Structure of Fin-Shock/Boundary-Layer Interactions by Laser Light-Screen Visualization

F. K. Lu and G. S. Settles,

Penn State University, University Park, PA

First Draft of a paper to be given at the First National Fluid Dynamics Congress, July 24-28, 1988, Cincinnati, Ohio

Structure of Fin-Shock/Boundary-Layer Interactions by Laser Light-Screen Visualization

F. K. Lu* and G. S. Settles†, Pennsylvania State University, University Park, PA, 16802

Abstract

The flowfield structure of fin-generated shock-wave/turbulent boundary-layer interactions at nominal Mach numbers of 2.5, 3, and 3.5 is studied using laser light-screen flow visualization. A sharp-leading-edged fin was used to generate swept planar shock waves which interacted with the 2-D, equilibrium turbulent boundary layer on an adiabatic flat plate. The shock wave strength was varied by adjustable fin angles up to 18°. The beam of a 4 W Argon-ion laser was expanded into a thin sheet and passed through the flow roughly normal to the interaction sweep line. Moisture in the airstream allowed the photography of interaction "slices." Quantitative data on the flowfield structures were obtained at Mach 3 and 3.5. Weak interactions appear nearly featureless, but distinct structural features appear and evolve as the shock strength is increased. An important discovery of this work is the flowfield structure downstream of the shock triple-point, which has not been properly observed before. A supersonic jet bounded by the slip line and flow separation zone is seen to curve downward and impinge on the flat plate. This phenomenon appears closely related to Edney-type leading-edge shock interference. Such structural features have not been resolved in previous flowfield surveys or Navier-Stokes solutions.

Nomenclature

M_∞ = incoming freestream Mach number
p_o = stagnation pressure of incoming stream, MPa (psia)
Re = unit Reynolds number, m^{-1} (/ft)
T_{aw} = adiabatic wall temperature, K (°R)
T_w = wall temperature, K (°R)
T_o = freestream stagnation temperature, K (°R)
α = angle made by fin with respect to the incoming freestream direction, deg.
β = angle made by surface-flow features or flowfield features projected onto the test surface, with respect to the incoming freestream direction, deg.
β_o = angle made by inviscid shock-wave trace on the test surface with respect to the incoming freestream direction, deg.
δ = local, undisturbed boundary-layer thickness, mm (in.)

Subscripts

A1 = primary flow attachment line (Figure 10)
B = top of separated boundary layer between S2 and S3 (Figure 6b)

---

* Graduate Research Assistant, Mechanical Engineering Department, presently, Assistant Professor, Aerospace Engineering Department, The University of Texas, Arlington, TX; Member AIAA.

† Associate Professor, Mechanical Engineering Department, Associate Fellow AIAA.

e = edge of vortical structure (Figure 6b)
h = height of flowfield feature above test surface, mm (in.)
l = distance of flowfield feature projected onto the test surface from the fin apex
p = intersection of the separation shock with the boundary layer (Figure 6b)
S2 = separation shock (Figure 6b)
S3 = internal shock (Figure 6b)
t = top of vortical structure (Figure 6b)
tp, TP = triple point of lambda shock structure (Figure 6b)
U = upstream influence line
ϕ = angle made by straightline segment of flowfield structure in the plane normal to the inviscid shock
∞ = incoming freestream conditions

Introduction

The problems of shock wave/boundary-layer interactions have been prominent in modern fluid dynamics for several decades. These problems not only pace the development of advanced computational and theoretical methods, but also have important relevance to high-speed flight. Numerous publications and several survey articles have appeared on the subject (see, e. g. , the recent review of swept interactions by Settles and Dolling[1]).

Most recently, shock wave/boundary-layer interaction problems have taken on added importance due to proposals for the development of a new generation of supersonic and hypersonic vehicles. Although these vehicles will likely be designed by computational methods, the lack of previous experience in computational hypersonics reduces confidence in its application.[2] This is especially so in the computation of complicated viscous-inviscid interacting flowfields such as that of a shock-wave/boundary-layer interaction[3] .

Thus, to support computational code validation and, more importantly, to understand the fluid-dynamic phenomena involved, recourse to experiments on shock/boundary-layer interactions is necessary. To meet the first goal, a broad and detailed database is called for in order to verify evolutionary efforts in code development. The second goal requires detailed experiments as well, but not always the same experiments. Exploratory studies aimed at revealing the interaction behavior, extent, and structure may be more useful than detailed quantitative measurements in satisfying this goal. Such experiments often should cover wide parametric ranges, say, of Mach and Reynolds numbers.

The present paper reports such an experimental study, aimed at understanding the *structure* of the interaction of a fin-generated, swept shock wave with a turbulent boundary layer. This basic research configuration, which is depicted in Figure 1, represents practically-occurring interactions on high-speed vehicles. Two examples are fin-fuselage junctions and corner flows in air inlets.

A key traditional question in all three-dimensional shock/boundary-layer interactions is the flowfield structure. For the often-studied fin case of Figure 1, previous experiments including detailed yaw-probe surveys[4-7] have provided some information regarding this structure, as sketched in Figure 2 (this sketch, from Reference 1, depicts the interaction flowfield in a plane normal to the inviscid shock). In interactions of sufficient strength, the incoming boundary layer is separated by a "separation shock" which is oblique to the

oncoming flow component in the normal plane. This shock is therefore relatively weak compared to the main, freestream shock. Hence another, downstream, shock is needed to turn the interacting flow in order to satisfy the boundary conditions imposed by the fin. This system of shock waves is similar to that seen in the more familiar case of the two-dimensional transonic shock/boundary layer interaction. When visualized using optical techniques, such a shock system appears to have a "λ" shape, hence the term *lambda-foot structure* is used to describe it. At the "triple point" of the lambda-foot, where the three shocks converge, a slip-surface forms. Across this surface, which appears as a line in the plane of Figure 2, pressure and flow direction must match but all other flow quantities may be discontinuous. Beneath the lambda-foot, the separated boundary layer rolls up into a flattened vortex as indicated in Figure 2. In some cases a secondary-separation vortex is suspected, although there is still insufficient direct evidence to support this.

While these flowfield features are relatively well-understood, what happens *downstream* of the lambda-foot is not so clear. Figure 2 shows an expansion and recompression based roughly on the inferences of previous investigators.[4,7] However, the phenomenology of this interaction region has not been clearly shown, either by previous flowfield surveys[1,4-6] or by computational simulations of the flowfield.[8] In all cases, insufficient resolution was obtained in previous studies to clearly portray the downstream structure. In the present work we will demonstrate by flow visualization that the earlier model of the downstream compression-expansion region, as shown in Figure 2, is incorrect.

Flowfield visualization is not new to shock/boundary-layer interactions. It has been applied in several previous studies.[9-14] Of these, References 9 through 11 used light-screen visualization, Reference 12 used the electron-beam technique, and References 13 and 14 used conical shadowgraphy. In general, the three-dimensional nature of swept interactions poses difficulty in applying classical optical techniques. However, for dimensionless fin-generated interactions, quasiconical symmetry[15] allows some simplification of both the experimental technique and the data analysis. Further, while most of the cited studies sought only qualitative flow visualization results, a proper analysis could have been used to extract quantitative information from the images obtained.[16] Finally, the previous applications of light-screen flow visualization to fin-generated shock-wave/boundary-layer interactions[9-11] shared the common problem of low contrast and resolution, making it very difficult to extract quantitative information from them.

Hence, to fulfill the need for a better understanding of the interaction flowfield structure, a new set of laser light-screen observations of fin-generated interactions has been performed and is reported here. The aims of this study are to examine the flowfield structure in detail, and to extract quantitative data on the key structural features from these observations. Before describing these experiments it is appropriate to briefly review the laser light-screen technique which they employed.

The Laser Light-screen Technique

Light-screen (also *light-sheet* and *vapor-screen*) flow visualization is a standard experimental technique originating from the early 1960's.[17] Though early difficulties were experienced in collimating non-coherent light, the recent availability of powerful laser sources now enables high-quality images to be obtained without undue difficulty. Usually the

flow is seeded with water vapor, either naturally or deliberately by injecting water into the airstream[18], though other seeding materials have been tried as well. Light is Mie-scattered by the aerosol particles as the flow passes through the light-screen.

Different scattering intensities thus indicate different flow densities, assuming that the aerosol was initially evenly-distributed in the flow. However, boundary-layers, if in contact with relatively hot surfaces, may re-evaporate condensing moisture, making interpretation of the results at such locations difficult. Further, a high-speed boundary-layer, being less dense than the freestream, contains a smaller particle number-density than the freestream. It is thus observed that such boundary-layers appear dark in light-screen images. Also, boundary-layer fluid which leaves the surface during flow separation appears dark as well.[17,18]

One drawback of the light-screen technique arises from condensing moisture in a supersonic stream, which adversely affects the flow.[19] For example, condensation shocks in the expansion of a supersonic wind tunnel nozzle are known to alter the flow properties, sometimes seriously. Many previous studies have used moist air with a frostpoint as high as $-4\,^{\circ}\mathrm{C}\,(25\,^{\circ}\mathrm{F})$, which jeopardizes the results due to the possibility of condensation shock formation.[19] The procedure we have followed to prevent this from happening is described in the next section.

The light-screen technique has been popular for visualizing the leeside flows over high-speed missiles and delta wings at angle-of-attack. For further details on the technique and such applications thereof in high-speed flows, the reader is referred to McGregor's original work[17] and the more recent contribution of Snow and Morris[18].

The Experiment

Wind Tunnel and Test Model

The Penn State Supersonic Wind Tunnel, used in this study, is a blowdown facility with a nominal Mach number range of 1.5 to 4. The variable Mach number capability is achieved by way of an asymmetric sliding-block nozzle. The test section of the wind tunnel is 150 mm (6 in.) wide, 165 mm (6.5 in.) high and 610 mm (24 in.) long.[21,22]

For the present experiments the interaction test surface (Figure 1) is a flat plate, 500 mm (19.5 in.) long, which spanned the test section. A fin model with a 10° sharp leading edge was placed with its tip 216 mm (8.5 in.) from the plate leading edge and 26.2 mm (1.03 in.) from the tunnel sidewall. The fin was 100 mm (4 in.) high, 127 mm (5 in.) long and 6.35 mm (0.25 in.) thick. The fin height of about 30δ ensured that the interaction was a semi-infinite one.[23] The length of the fin was chosen to provide the maximum interaction extent while allowing sufficiently large angles-of-attack to be obtained without stalling the wind tunnel. Further, the height-to-length ratio ensured that disturbances from the top of the fin leading edge passed behind the test region.

The fin was held tightly onto the flat plate by a fin-injection mechanism mounted on the tunnel sidewall. The bottom of the fin had a rubber seal which ensured that no leakage under the fin occurred during the tests. Once test conditions were established, the fin-injection mechanism pneumatically injected the fin to a preset angle-of-attack, α. This was necessary only for tests with α larger than approximately 14°. At lower angles, α was

fixed before the run. The fin angle was determined to 0.1° accuracy using a machinist's protractor.

Test Conditions

The experiments were performed with freestream Mach numbers of 2.47, 2.93, and 3.44. The initial conditions of the incoming freestream at these Mach numbers are summarized in Table 1.

The undisturbed flat-plate boundary-layers at these Mach numbers have been surveyed and documented[22]. These boundary-layers are turbulent and in equilibrium in the sense that they satisfy the combined law-of-the-wall/law-of-the-wake with constant wake-strength parameter within the accepted equilibrium range. The test boundary-layers are also near-adiabatic ($T_w/T_{aw} \approx 1.04$). Example velocity profiles across the undisturbed boundary-layers at the two higher Mach numbers are shown in Figures 3a and 3b, along with the corresponding Sun-Childs[24] wall-wake curvefits to the data. The surveys along the flat-plate centerline and 38 mm (1.5 in.) to each side showed that the test boundary-layers are two-dimensional.

The dewpoint (or, more correctly, the frost point) of the air in the storage tank for the present experiments was kept to $-14 \pm 2\,^{\circ}\mathrm{C}$ ($6 \pm 5\,^{\circ}\mathrm{F}$), measured when the storage-tank pressure was 1.4 MPa (200 psia). This dewpoint results in an error due to moisture condensation of less than one percent of the freestream static pressure, or the freestream Mach number, for the Mach number range of the present experiments.[21,22] This amount of water vapor was also sufficient to yield good light-screen images. In order to achieve this moisture level, the air, after being compressed, is sent directly to the storage tank without passing through the normal drying equipment. Experience with the Penn State Supersonic Wind Tunnel reveals that the residual amount of water vapor in the air after compression results in a dewpoint of about $-14^{\circ}C$.

Discrete fin angles-of-attack were set at $\alpha = 7°$, 10°, 15° and 18°. However, at $M_\infty = 2.47$, the $\alpha = 18°$ case was found to cause tunnel stalling and was thus eliminated from the test matrix.

Optical Equipment

The experimental optical setup for laser light-screen imaging is diagrammed in Figure 4. The collimated beam of a 4 W Argon-ion laser is reflected from two steering mirrors, $SM1$ and $SM2$, before passing through a cylindrical lens which spreads the beam into a sheet of light 1.2 mm (0.05 in.) thick. The steering mirrors allow for quick and easy adjustment of the beam. By rotating mirror $SM1$ and translating and rotating mirror $SM2$, the light-screen could be positioned accurately within limits imposed by the 300 mm (6 in.) mirror diameters.

The light-screen was photographed by an Olympus OM-2S camera with a Vivitar 28-90 mm macrofocusing zoom lens combined with a Vivitar 2× macrofocusing teleconverter. Photographs were taken automatically and were bracketed by ±2/3 and ±4/3 stops, yielding five photographs per test run. Using Kodak TMAX ISO-400 film, the optimum exposure time was found to be in the range of 1/15 to 1/30 second.

To provide a reference, a "tare" photograph was taken of a grid of 2.54 mm (0.1 in.) squares. This grid was positioned to coincide with the light-screen plane in the wind tunnel test section. During subsequent data reduction the geometry of the flow structures was obtained, through triangulation, by referring to the tare photograph.

The fin and flat plate were painted flat-black to reduce stray reflections. Nonetheless, with the light-screen incident on the fin, reflected light caused photographs from the initial experiments to have poor contrast. This situation was remedied by passing the light-screen about 5 mm (0.25 in) to the rear of the fin. Most of the incident laser light, then reflected from the far wall of the wind tunnel, no longer entered the camera lens (Figure 5). This orientation of the light-screen, however, prevented it from being exactly normal to the undisturbed fin shock wave, so that a further correction was required in the data reduction. Finally, the camera was positioned approximately normal to the light-screen in order to capture as much side-scattered light as possible.

The results of the experiments, a set of photographic negatives, were printed on high-contrast photographic paper. A selection of these results was then digitized using a high-resolution video camera feeding a Quantex QX-9210 digital image processor. Contrast enhancement and psuedocolor encoding were performed on the 480 × 640-pixel digitized images. Though not attempted thus far, it appears possible to correlate the digitized image brightness level with the flow density, utilizing the known flow density levels before and after the fin shock as reference conditions.

Results

Qualitative Analysis

Based on Korkegi's well-known separation criterion,[25] incipient three-dimensional turbulent boundary-layer separation occurs at Mach 2.5, 3, and 3.5 for shock waves generated by $\alpha = 7°$, 6°, and 5° fins, respectively. Therefore the present results are generally expected to involve boundary-layer separation, which is likely to be quite strong for the larger fin angles.[1,5-9,13-15,21-23] One thus expects to observe flowfield features similar to those sketched in Figure 2. To illustrate this point, Figure 6a presents a digitally-enhanced photograph of the light-screen visualization obtained at Mach 3.5 with an $\alpha = 10°$ fin. The essential features are labelled in the schematic sketch shown in Figure 6b.

The photograph of Figure 6a reveals that the freestream shock $S1$ is curved just above the triple-point, TP. (Wide-field photographs show that $S1$ is eventually straight further away from its interaction with the boundary-layer.) The incoming boundary layer, BL, separates beneath the initial oblique separation shock, $S2$, according to the accepted flowfield model. The separation shock compresses and slows the streamtube subtended by the points SP and TP. The internal or rear shock, $S3$, is also obvious in the light-screen image. Thus, the well-known lambda-foot structure of shock-induced boundary-layer separation, as described previously, can be clearly seen in the present results typified by Figure 6a. However, no clear structure is visible in the photograph *downstream* of the lambda-foot (that is, to the left of it in Figure 6a). Our contention, elaborated below, is that a definite structure is present but too weak *in this example* to be visible.

Shock waves $S2$ and $S3$ are essentially straight, as is the "top" of the boundary layer between SP and ST. Thus the angles ϕ_{S2}, ϕ_{S3} and ϕ_B, in the plane normal to the

inviscid freestream shock, can be defined for these features and can be extracted from the light-screen photographs in the form of quantitative data.

At $M_\infty = 3.5$ and with α increased to 15°, flowfield structural features *downstream* of the lambda-foot are now strong enough to be visible in the laser light-screen image (Figure 7a). In particular, a curved line (presumably the slip-line) emanates from the triple-point and impinges on the flat plate. A high brightness (density) level is obvious between the slip line and the dark boundary-layer separation region. Further, striations are visible normal to the curved boundaries of this downstream flow region. These features are also visible in photographs taken at $M_\infty = 3.5$ and $\alpha = 18°$. Prior evidence of the structure revealed here in the interaction flowfield downstream of the lambda-foot is known to the authors from Mach 6 interaction light-screen photographs by T. J. Goldberg of NASA-Langley Research Center. Goldberg's work remains unpublished, but was sketched and briefly discussed by Oskam, et. al.[11]

Figure 7a is highly reminiscent of the leading-edge shock interference phenomenon pioneered by Edney.[26] It resembles a "Type IV" shock interference Edney's parlance, which is an interference resulting in a supersonic jet impingement upon the adjacent surface (see Figure 8). By analogy with Edney's results, this jet-impingement phenomenon is believed to shed new light on the high surface heating rates which have been observed near flow reattachment in separated, swept shock/boundary-layer interactions.[27]

Specifically, based on the above observations, we propose a revised model for the interaction structure downstream of the lambda-foot. Instead of the previous model shown in Figure 2, that of Figure 7b now appears more reasonable. The streamtube that is processed through lambda-shocks $S2$ and $S3$ is bounded downstream by the slip-line "e" (above) and the vortical separation region "h" (below). This streamtube is forced to bend downward toward the test surface by the high pressure in region "n" after the inviscid shock "c." Prandtl-Meyer expansion fans "f" accelerate the streamtube toward the surface in the form of a supersonic jet. Finally, a normal-shock "g" occurs just above the impingement of the jet upon the test surface in the vicinity of the flow attachment line "l."

The new interaction structure model of Figure 7b is presently supported only for strong interactions with significant three-dimensional boundary-layer separation. For those weaker interactions in the present test matrix, the photographic light-screen results do not clearly show any downstream structure. However, direct visual observations of the light-screen during the experiments did reveal the slip-line shape shown in Figure 7b in the much weaker interaction at $M_\infty = 3$ and $\alpha = 10°$. This is in direct contrast to the previous interpretation by Oskam, et. al.[4] of his flowfield survey results from the same interaction. (Oskam concluded that the boundary-layer did not separate.) We believe that the available flowfield survey data are of insufficient resolution to reveal the features shown in Figures 7a and 7b, or, for that matter, to reveal boundary-layer separation. For the record, the available Navier-Stokes solutions for these interactions, typified in Reference 8, similarly fail to resolve the flowfield structure because of insufficient grid resolution.

Finally, Figure 9 shows an additional light-screen image for the weak interaction case of $M_\infty = 2.5$ and $\alpha = 10°$. Here, the curvature of the fin shock is still seen but its bifurcation into a lambda-foot is quite weak. From an examination of Figures 6a, 7a, and 9, one observes that the rear leg of the lambda-foot rotates downstream (clockwise) as the

interaction strength increases, thus decreasing the angle ϕ_{S3}. It further appears from this comparison that the interaction flowfield structure is a strong function of the interaction strength, that is, the degree of boundary-layer separation. These qualitative observations are pursued further in the discussion which follows.

Quantitative Analysis

Previous studies[1,6,13,15,21,23] have shown that the swept-interaction flowfield, away from an inception region near the fin tip, appears to grow conically from a virtual origin. This principle was dubbed *quasiconical interaction symmetry* by its originators.[15] Figure 10 illustrates this concept in terms of features observed in earlier surface-flow visualization[21] experiments. For the present experiments, quasiconical symmetry is exploited in the data analysis. The points SE, ST, SP and TP of Figure 5b are projected onto the flat plate from the light-screen photographs, whence the angles of these features with respect to the flow direction can be measured. (The angular reference scheme is diagrammed in Figure 11.) For simplicity, these measurements are referenced to the fin leading-edge rather than the true conical-flow virtual origin, which introduces a certain error. This error is believed to be generally comparable to the angular accuracy limit of about $\pm 1.5°$ due to the resolution of the light-screen photographs. In some cases, however, the leading-edge-origin simplification may lead to more serious errors.

The separation shock $S2$ is used to illustrate how ϕ_{S2}, ϕ_{S3} and ϕ_B are determined. $S2$ intersects the flat plate at C in the plane of the lightsheet $P1$. In the plane normal to the inviscid shock, $P2$, $S2$ intersects the flat plate at C', yielding $\angle BC'A = \phi_{S2}$. Let $AB = h_{tp}$ and $AO = l_{tp}$. The line OCC' makes an angle ϵ with respect to the incoming freestream. Note that $P1$ and $P2$ intersect along AB. Therefore, from trigonometry,

$$\phi_{S2} = \arctan\left[\frac{h_{tp}}{l_{tp}\tan(\epsilon - \beta_{tp})}\right] \tag{1}$$

In general, any straight-line segment can be resolved in a similar manner, so that

$$\phi = \arctan\left(\frac{h}{l\tan|\epsilon - \beta|}\right) \tag{2}$$

The absolute value $|\epsilon - \beta|$ is used here so that $\phi < 90°$.

Angular Characterization of Interaction Structure

Having used the preceding analysis to extract quantitative information from the laser light-screen results at Mach 2.95 and 3.44, we may now examine certain aspects of the interaction structure. Note that, according to the principle of quasiconical interaction symmetry, it makes no sense to characterize the structure in terms of either spatial positions or length dimensions. Only *angles* are necessary or desirable for such a description.

The angle made by the downstream edge of the separated, vortical region with respect to the incoming freestream direction, β_e, is plotted against the fin angle, α, in Figure 12. Also plotted for comparison in Figure 12 is the attachment-line angle, β_{A1}, obtained from

previous surface-flow visualization results.[21,22] It can be seen that β_e is slightly smaller than β_{A1} at both Mach numbers, though these two angles exhibit similar trends with α. The error incurred earlier in approximating the virtual conical origin by the fin leading-edge position in determining β_e is believed to be responsible for this discrepancy. Physically, $\beta_e \geq \beta_{A1}$ would be expected.

Next, the intersection of the separation shock with the boundary layer makes an angle β_p with the freestream, when projected onto the test surface (see Figure 11) The angle β_p is plotted in Figure 13 against α. Also shown for comparison in the Figure is the upstream-influence angle, β_U, reported previously.[21] It can be seen from this plot that, within the data scatter,

$$\beta_p = \beta_U$$

Thus, one may conclude that the upstream-influence line coincides with the origin of the compression system which becomes the separation shock-wave. This makes physical sense, and has been observed often in *two-dimensional* interactions by comparing schlieren photos and wall pressure distributions.

The triple-point of the lambda-foot shock structure is usually assumed to be coplanar with the undisturbed, inviscid shock wave. However, in view of the shock curvature discussed earlier, this cannot be strictly true. Figure 14 reveals this by comparing the growth of the projected triple-point angle on the test surface, β_{tp}, with the inviscid-shock angle β_o. At both Mach 2.93 and 3.44 the triple-point is from 0.5 to 2° ahead of the inviscid shock. Further, Figure 14 indicates that the triple-point angle approaches the inviscid shock angle with increasing shock strength (meaning that the inviscid shock curvature is reduced). The physical explanation of this is not immediately obvious.

Finally, the separation-shock angle ϕ_{S2} is plotted versus fin angle α in Figure 15. A dramatic decrease in ϕ_{S2} is seen as the interaction grows stronger. Physically, this corresponds to a stretching of the interaction "footprint" over a wider angular spread. Assuming locally two-dimensional flow in the plane normal to the inviscid shock, ϕ_{S2} is specified if ϕ_B and the normal component of freestream Mach number are known. There is previous evidence from free-interaction arguments and supporting experiments that the flow separation angle ($\approx \phi_B$) remains relatively fixed between about 8° and 12° in many two- and three-dimensional supersonic interactions.[1] Thus, the observed decrease of ϕ_{S2} in Figure 15 appears to be due primarily to the increase of the normal component of freestream Mach number with increasing α.

Conclusions

In summary, this flow-visualization study has examined the structure of fin-generated shock-wave/turbulent boundary-layer interactions over ranges of both Mach number and interaction strength. The resulting laser light-screen images have permitted a clear observation of the interaction structure as well as the extraction of quantitative data on structural features. Several observations and conclusions have been drawn from this study. Principally, it has been shown that a previously unknown jet-impingement structure exists downstream of the familiar lambda-shock of well-separated interactions. This suggests the phenomenological reason for the high heat transfer rates observed by others in the flow reattachment region, in direct analogy with the problem of leading-edge shock wave

interference. By contrast, however, weaker interactions without significant flow separation appear relatively featureless except for a noticeable curvature of the main shock wave. Previous interaction studies involving both flowfield surveys and Navier-Stokes computations have failed to resolve the structural features observed here by optical means.

Acknowledgments

This research was supported by AFOSR Grant 86-0082 from the U. S. Air Force Office of Scientific Research, monitored by Dr. J. D. Wilson, and by Joint Research Interchange NCA2-192 with the NASA Ames Research Center, in which Dr. C. C. Horstman was the research collaborator.

References

1. Settles, G. S. and Dolling, D. S., "Swept Shock Wave/Boundary-Layer Interactions," in *AIAA Progress in Astronautics and Aeronautics: Tactical Missile Aerodynamics*, edited by M. Hemsch and J. Nielsen, Vol. 104, AIAA, New York, 1986, pp. 297-379.

2. Anderson, J. D., Jr., "A Survey of Modern Research in Hypersonic Aerodynamics," AIAA Paper 84-1578, June 1984.

3. Horstman, C. C., "Prediction of Hypersonic Shock-Wave/Turbulent-Boundary-Layer Interaction Flows," AIAA Paper 87-1367, June, 1987.

4. Oskam, B., "Three-Dimensional Flow Fields Generated by the Interaction of a Swept Shock Wave with a Turbulent Boundary Layer," Ph.D. Thesis, Princeton University, September 1976.

5. Peake, D. J., "The Three-Dimensional Interaction of a Swept Shock Wave with a Turbulent Boundary Layer and the Effects of Air Injection on Separation," Ph.D. Thesis, Carleton University, Canada, March 1975.

6. Kimmel, R. L., "An Experimental Investigation of Quasi-Conical Shock Wave/-Turbulent Boundary Layer Interactions," Ph.D. Thesis, Princeton University, June 1987.

7. Zheltovódov, A. A., "Regimes and Properties of Three-Dimensional Separation Flows Initiated by Skewed Compression Shocks," *Zhurnal Prikladnoi Mekhaniki i Tekhnicheskoi Fiziki*, No. 3, May-June 1982, pp. 116-123.

8. Knight, D. D., Horstman, C. C., and Shapey, B. L. "The Flowfield Structure of the 3-D Shock Wave-Boundary Layer Interaction Generated by a 20 Degree Sharp Fin at Mach 3," AIAA Paper 86-0343, January, 1986.

9. Kubota, H., "Investigations of Three-Dimensional Shock Wave Boundary Layer Interactions," Ph.D. Thesis, Cranfield Institute of Technology, January 1980.

10. Rao, D. S., Private Communication in Peake, D. J. and Tobak, M., "Three-Dimensional Interactions and Vortical Flows with Emphasis on High Speeds," NASA TM 81169, March 1980.

11. Goldberg, T. J., Private Communication in Oskam, B., Vas, I. E. and Bogdonoff, S. M., "Mach 3 Oblique Shock Wave/Turbulent Boundary Layer Interactions in Three Dimensions," AIAA Paper 76-0336, January 1976.

12. Watson, R. D., "Experimental Study of Sharp- and Blunt-Nose Streamwise Corners at Mach 20," NASA TN D-7398, April 1974.

13. Zubin, M. A. and Ostapenko, N. A., "Structure of Flow in the Separation Region Resulting from Interaction of a Normal Shock Wave with a Boundary Layer in a Corner," *Izvestiya Akademii Nauk SSSR, Mekhanika Zhidkosti i Gaza*, Vol. 14, May-June 1979, pp. 51-58.

14. Settles, G. S. and Teng, H.-Y., "Flow Visualization Methods for Separated Three-Dimensional Shock Wave/Turbulent Boundary Layer Interactions," *AIAA Journal*, Vol. 21, March 1983, pp. 390-397.

15. Settles, G. S. and Lu, F. K., "Conical Similarity of Shock/Boundary-Layer Interactions Generated by Swept and Unswept Fins," *AIAA Journal*, Vol. 23, No. 7, pp. 1021-1027, July 1985.

16. O'Hare, J. E., "Digital Image Analysis for Aerodynamic Testing," in *Proceedings of the 27th Symposium of ISA*, Vol. 18, Part One, 1981.

17. McGregor, I., "Development of the Vapour Screen Method of Flow Visualization in a 3 ft $\times$3 ft Supersonic Tunnel," in AGARDograph 70, *Flow Visualization in Wind Tunnels Using Indicators*, compiled by R. L. Maltby, April 1962.

18. Snow, W. L. and Morris, O. A., "Investigation of Light Source and Scattering Medium Related to Vapor-Screen Flow Visualization in a Supersonic Wind Tunnel," NASA TM 86290, 1984.

19. Wegener, P. P. and Mack, L. M., "Condensation in Supersonic and Hypersonic Wind Tunnels," *Advances in Applied Mechanics*, Vol. V, edited by H. L. Dryden and Th. von Kármán, Academic Press, New York, 1958, pp. 307-447.

20. Monaghan, R. J., "Tests of Humidity Effects on Flow in a Wind Tunnel at Mach Numbers between 2.48 and 4," British A.R.C. CP No. 247, January 1955.

21. Lu, F. K., Settles, G. S. and Horstman, C. C., "Mach Number Effects on Conical Surface Features of Swept Shock Boundary-Layer Interactions," AIAA Paper 87-1365, June 1987.

22. Lu, F. K., "Mach Number Effects on Fin-Generated Shock-Wave Boundary-Layer Interactions," Ph.D. Thesis, The Pennsylvania State University, to be published.

23. McClure, W. B., "An Experimental Study into the Scaling of the Interaction of an Unswept Sharp Fin-Generated Shock/Turbulent Boundary Layer Interaction," M.S.E. Thesis, Princeton University, January 1983.

24. Sun, C. C. and Childs, M. E., "A Modified Wall-Wake Velocity Profile for Turbulent Compressible Boundary Layers," *AIAA Journal of Aircraft*, Vol. 10, June 1973, pp. 318-383.

25. Korkegi, R. H., "A Simple Correlation for Incipient Turbulent Boundary-Layer Separation due to a Skewed Shock Wave," *AIAA Journal*, Vol. 11, November 1973, pp. 1578-1579.

26. Edney, B. E., "Anomalous Heat Transfer and Pressure Distributions on Blunt Bodies at Hypersonic Speeds in the Presence of an Impinging Shock," FFA Report 115, The Aeronautical Research Institute of Sweden, Stockholm, Sweden, February 1968.

27. Neumann, R. D., and Hayes, J. R., "Introduction to Aerodynamic Heating Analysis of Supersonic Missiles," in *AIAA Progress in Astronautics and Aeronautics: Tactical Missile Aerodynamics*, edited by M. Hemsch and J. Nielsen, Vol. 104, AIAA, New York, 1986, pp. 421-481.

Table 1 Incoming Freestream Conditions

M_∞	p_o, MPa (psia)	T_o, K (°R)	$Re \times 10^{-6}$, m^{-1} (/ft)
$2.47 \pm 0.1\%$	$0.54 \pm 2.0\%$ (78)	$295 \pm 0.9\%$ (531)	$53.8 \pm 0.9\%$ (16.3)
$2.95 \pm 0.3\%$	$0.76 \pm 2.7\%$ (110)	$295 \pm 0.9\%$ (531)	$58.9 \pm 1.9\%$ (17.8)
$3.44 \pm 0.2\%$	$1.03 \pm 3.0\%$ (150)	$295 \pm 0.8\%$ (531)	$64.0 \pm 1.7\%$ (19.4)

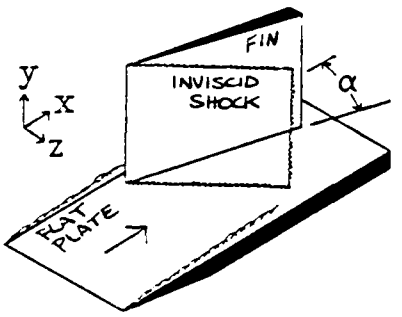

SHARP UNSWEPT FIN

Figure 1 - Test Geometry

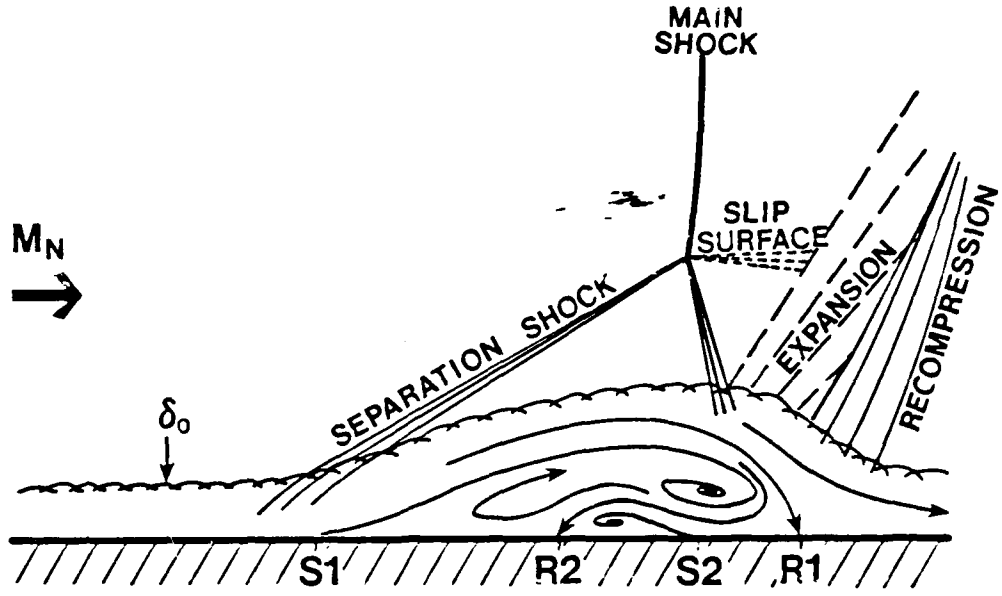

Figure 2 - Previous Interaction Flowfield Model

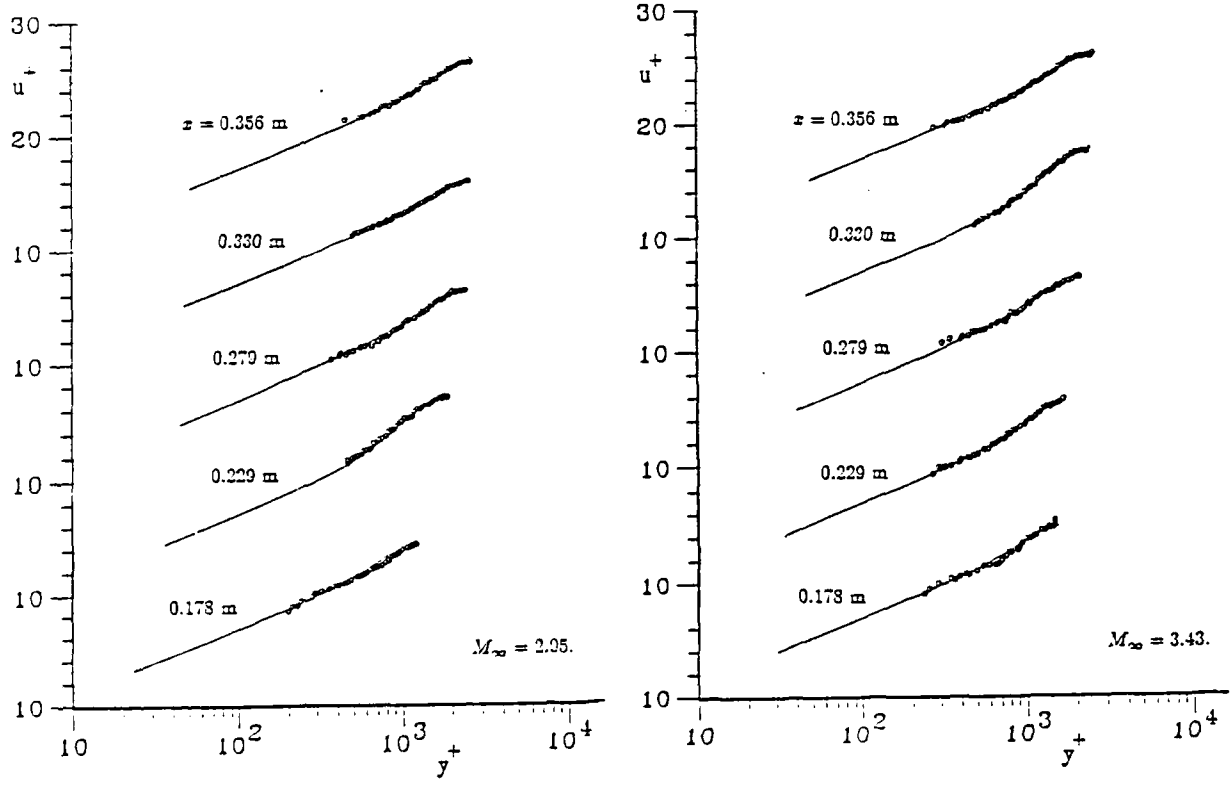

Figure 3. Velocity profiles of undisturbed boundary layers in wall coordinates

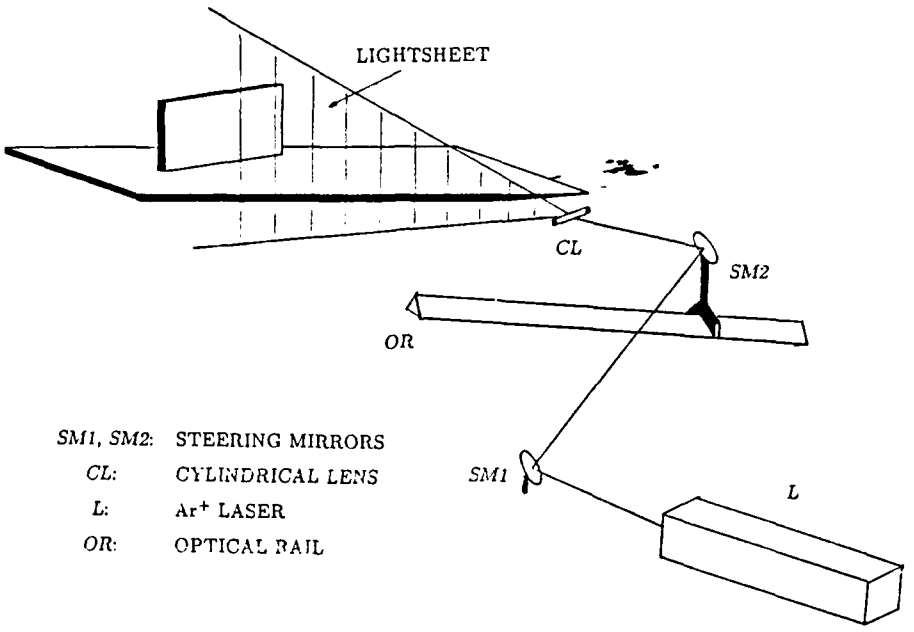

Figure 4. Experimental setup for laser lightsheet flow visualization.

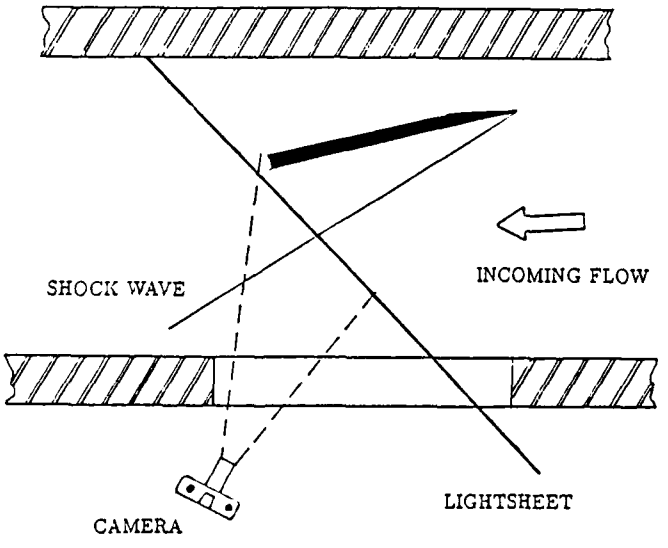

Figure 5 . Technique for improving image contrast in the laser lightsheet experiments. (TOP VIEW)

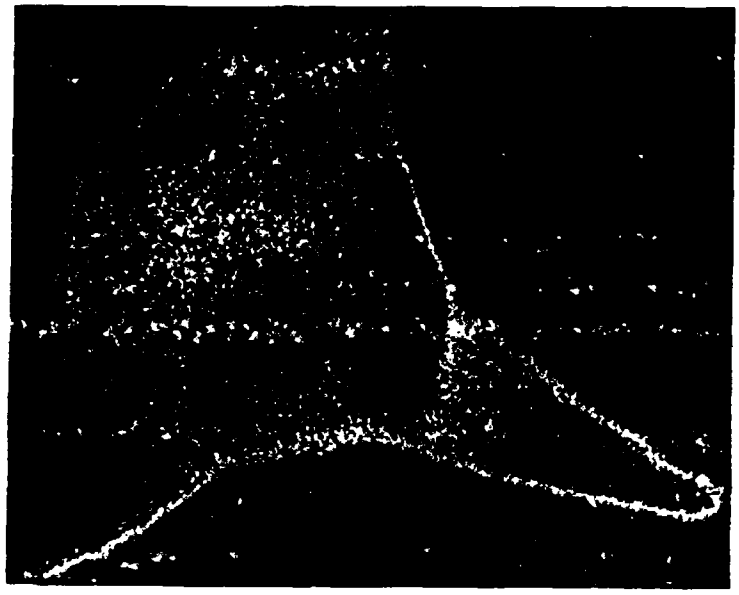

Figure 6a - Example Light-Screen Photo (Mach 3.44, alpha = 10 deg.)

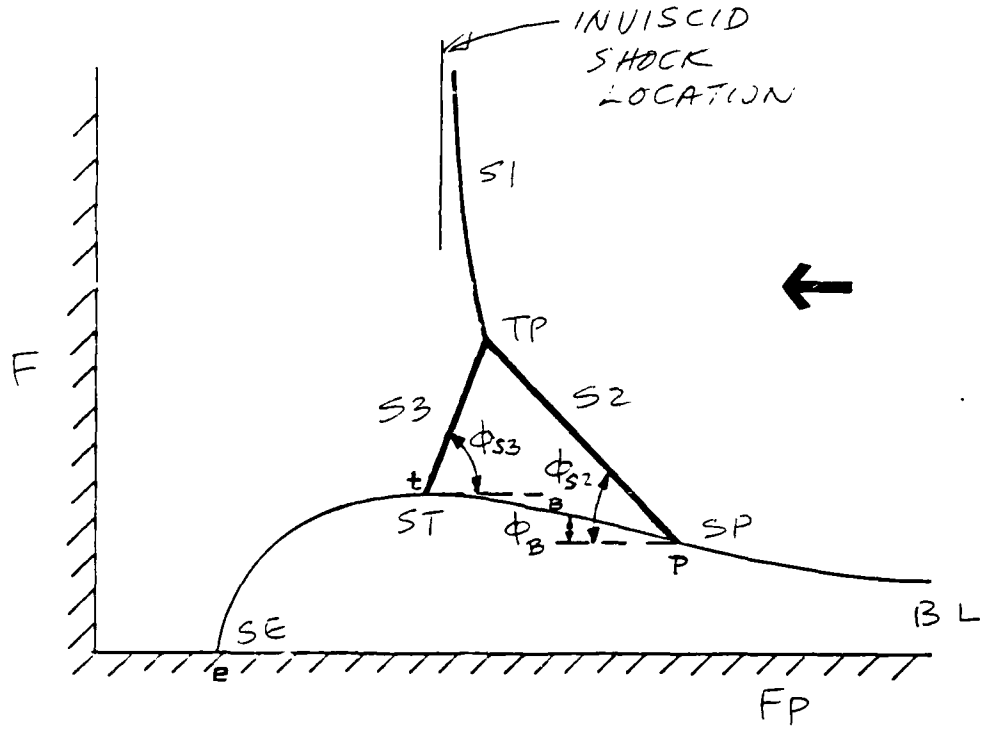

Figure 6b - Diagram of Main Features of Interaction in Crossflow Plane

S1 = main shock
S2 = separation shock
S3 = internal shock
BL = incoming boundary layer
ST = top of separated region
SE = inner edge of separated region
SP = intersection of S2 w/BL
TP = triple point
F = fin
FP = flat plate

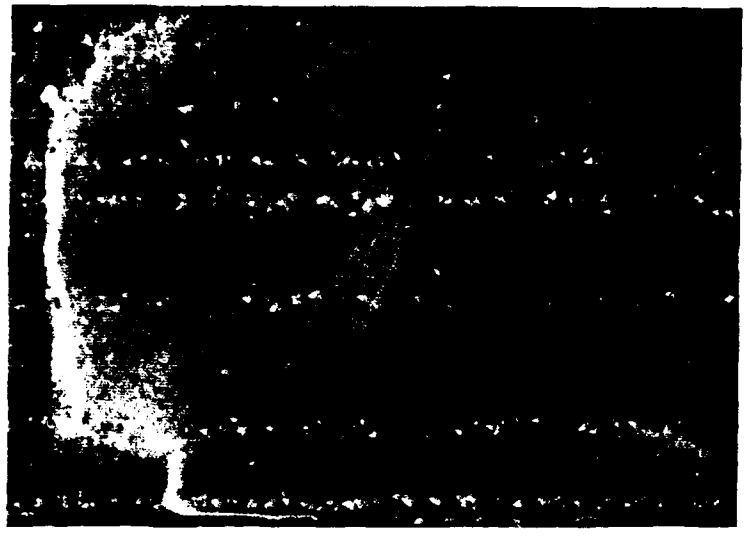

Figure 7a- Light-Screen Photo of Interaction Structure, Mach 3.44, alpha = 15 deg.

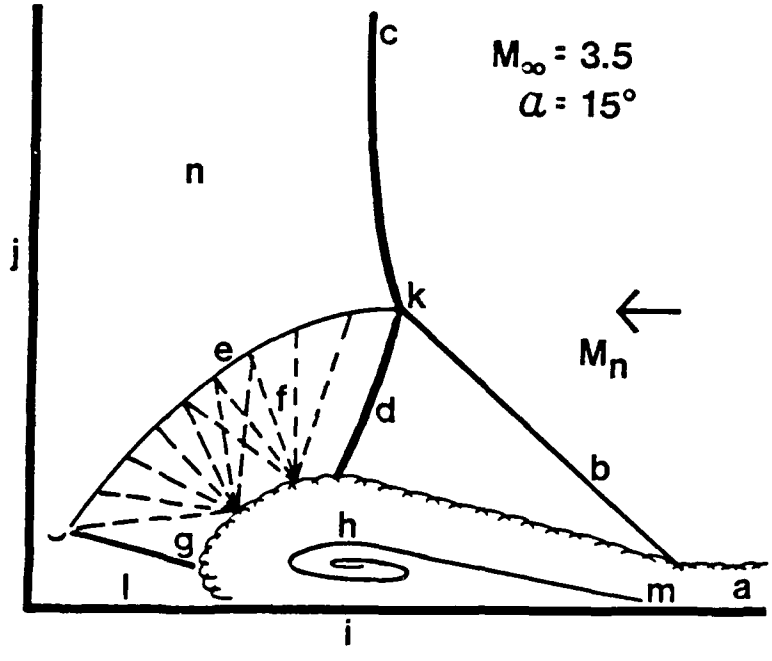

Figure 7b - Diagram of Interaction Structure

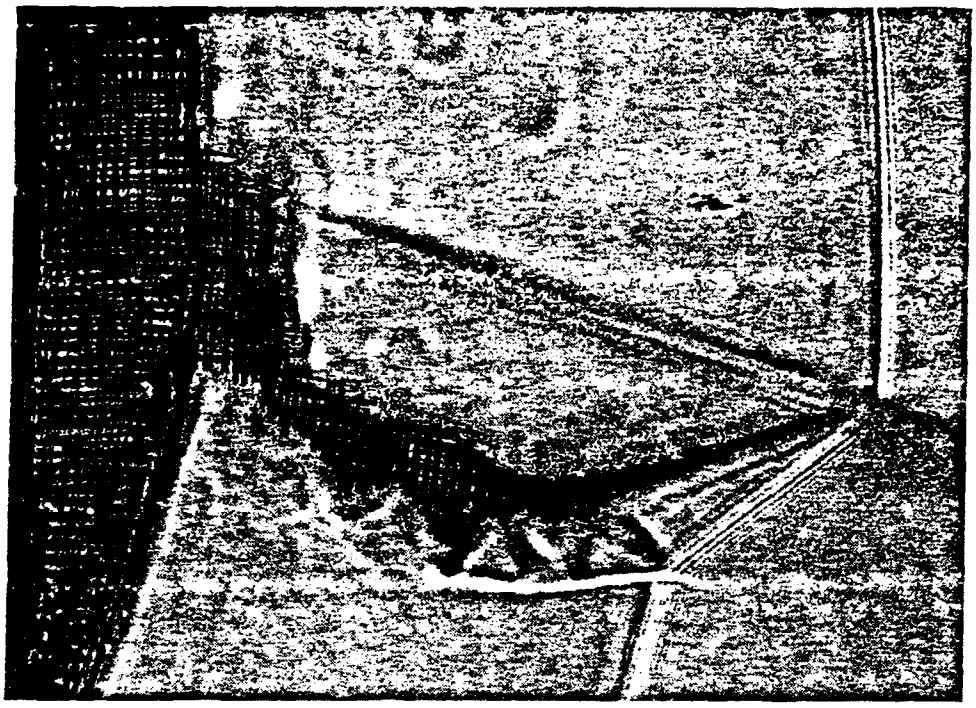

Figure 8 - Leading-Edge Shock Interference with Jet Impingement
(Photo by B. Edney)

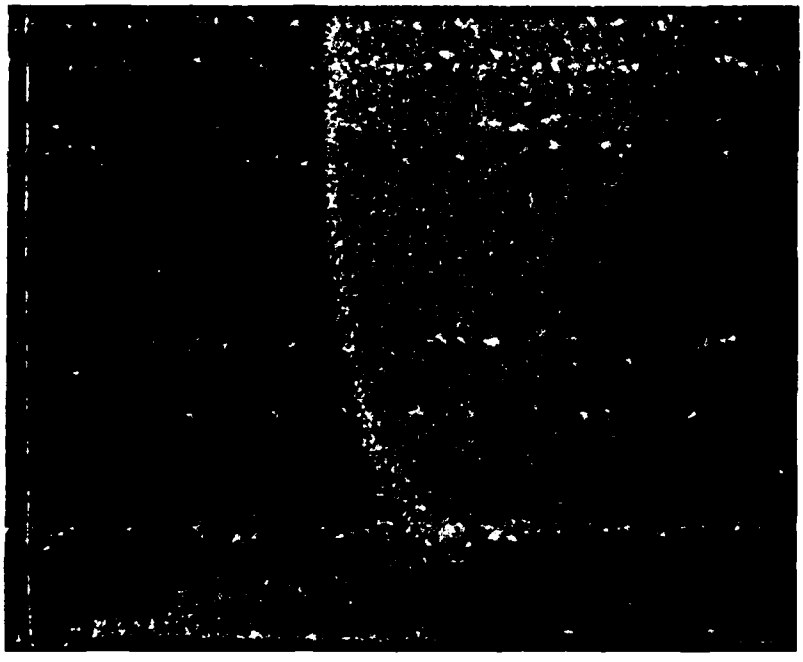

Figure 9 - Light-Screen Photo of Weak Interaction (Mach 2.47, alpha=10 deg.)

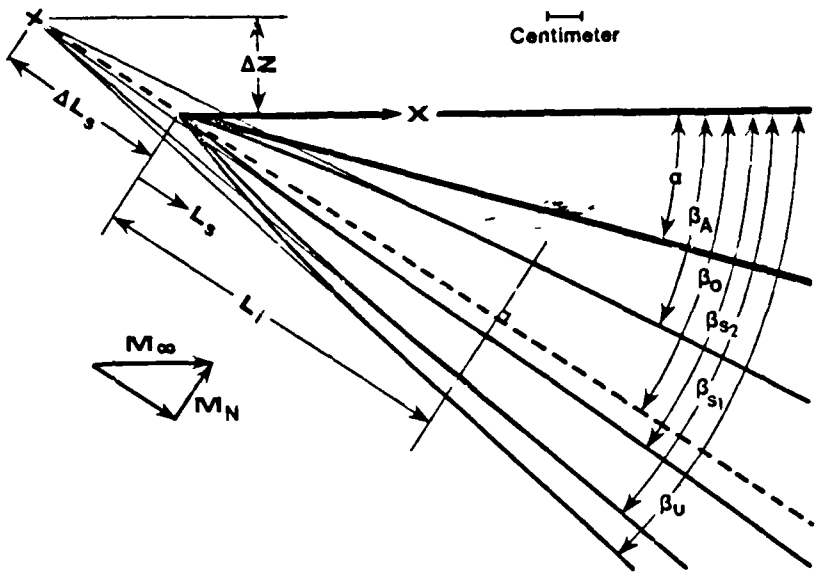

Figure 10 - Diagram of Quasiconical Fin Interaction Surface Flow Pattern

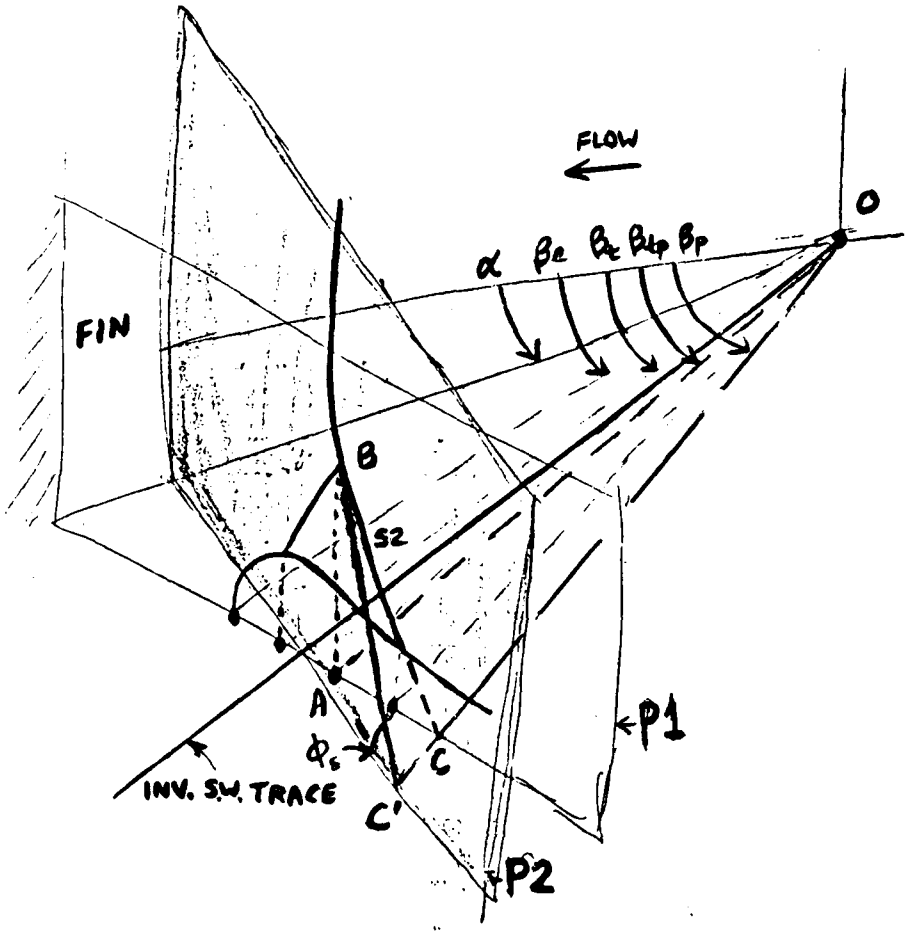

Figure 11 - Angular Reference Scheme of Interaction Features in Planes P1 and P2, Projected on Test Surface

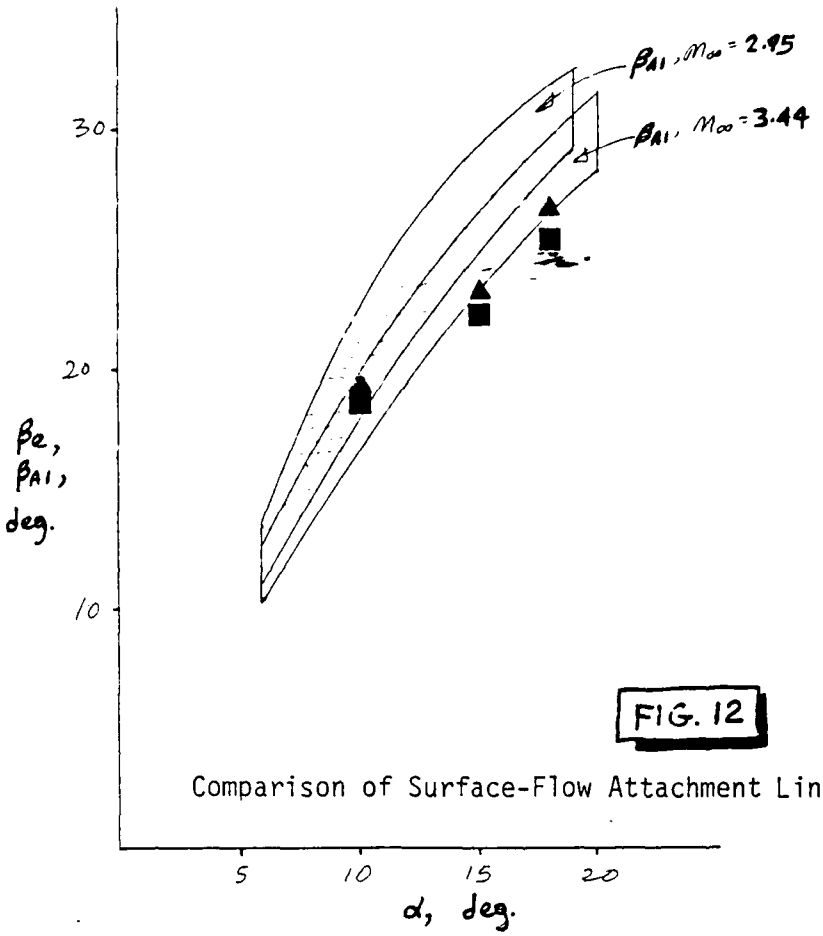

FIG. 12

Comparison of Surface-Flow Attachment Line & Light-Screen

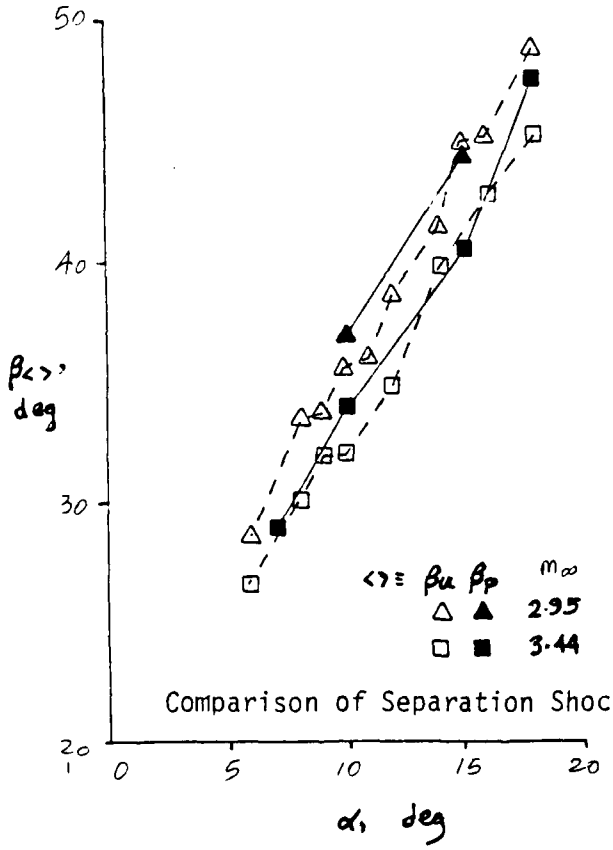

FIG. 13

Comparison of Separation Shock Origin & Upstream Influence

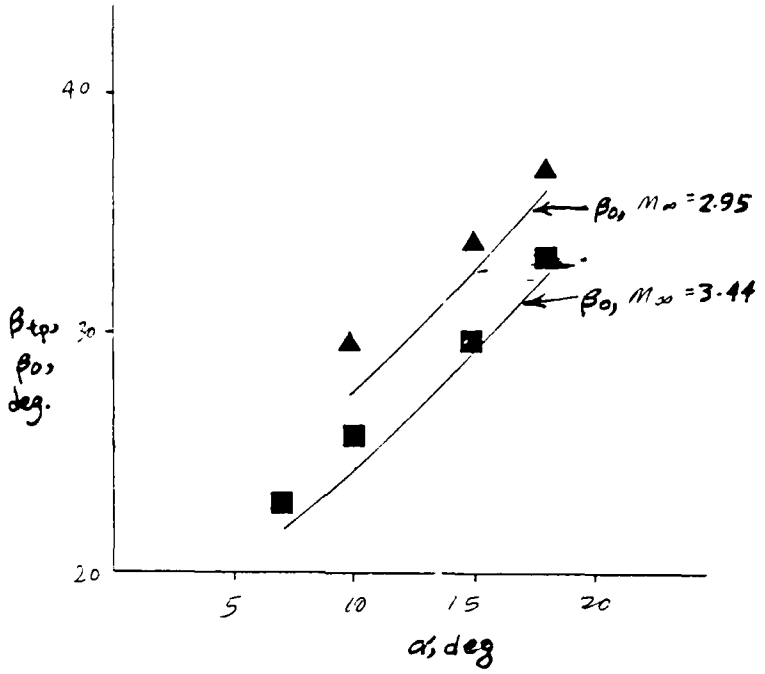

Figure 14 - Triple-point Angle Compared to Undisturbed Main Shock Angle

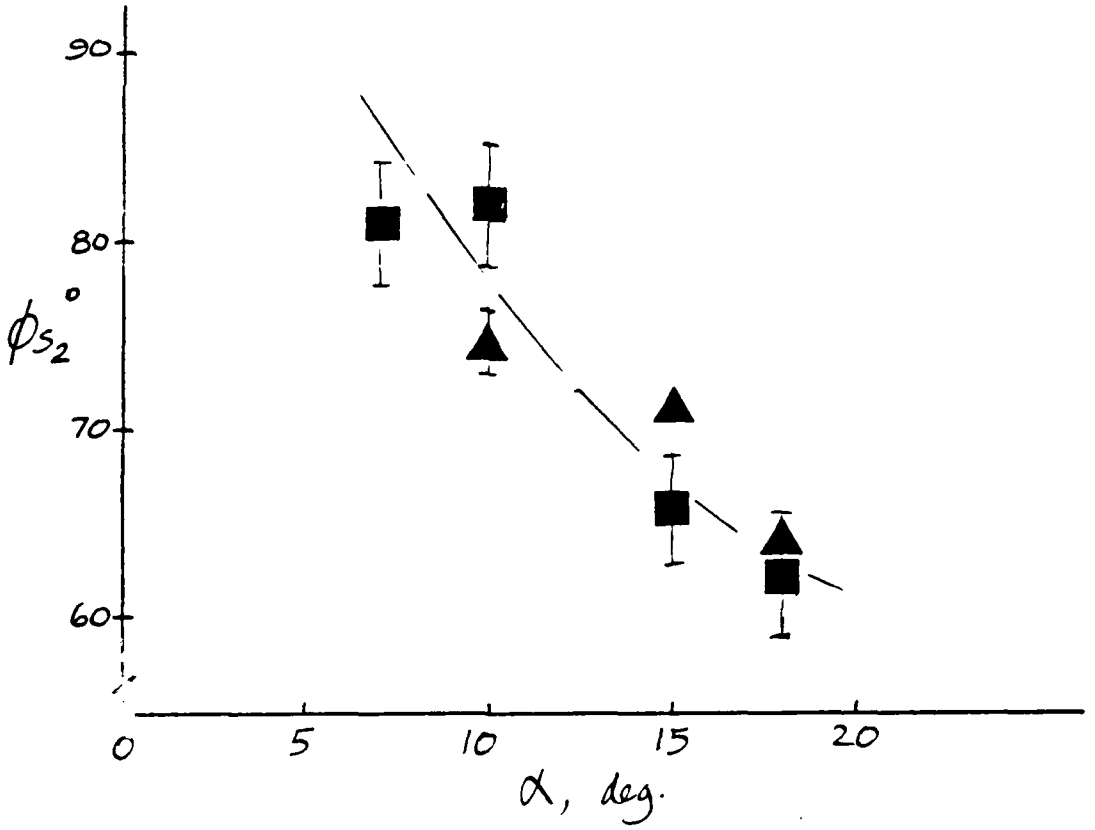

Figure 15 - Trend of Separation-Shock Angle with Interaction Strength

AIAA'88

XI. Appendix B

AIAA-88-0497

Skin Friction Measurements by Laser Interferometry in Swept Shock Wave/ Turbulent Boundary-Layer Interactions

K.-S. Kim and G. S. Settles,

Penn State University, University Park, PA

AIAA 26th Aerospace Sciences Meeting

January 11-14, 1988/Reno, Nevada

Skin Friction Measurements by Laser Interferometry in Swept Shock Wave/Turbulent Boundary-Layer Interactions

Kwang-Soo Kim* and Gary S. Settles†, Pennsylvania State University, University Park, PA, 16802

Abstract

Experimental measurements have been made of wall shear stresses in swept interactions of a planar shock wave generated by a fin at angle of attack, and the two-dimensional turbulent boundary layer on a flat plate. Test conditions were: Mach number 3.03, Reynolds number $Re_\theta = 14915$, wall temperature near adiabatic, and fin angles 10° and 16°. Measurements were made using the Laser Interferometer Skin Friction (LISF) Meter, which optically detects the rate of thinning of an oil film applied to the test surface. The results show that such measurements are practical in high-speed interacting flows, and that a repeatability of ±6% or better is obtainable. Further, with proper data acquisition and reduction, LISF measurements appear feasible at very high wall shear levels which were previously considered unobtainable. Dramatic increases in wall shear were observed in both swept interactions tested. Data obtained along conical rays agree with the quasiconical interaction model proposed previously. The data are compared with the computational Navier-Stokes solutions of Horstman and Knight, wherein k-ϵ and algebraic eddy-viscosity turbulence models were used, respectively. Both computations simulate some features of the measured c_f distributions but fail to predict other features properly.

Nomenclature

c_f	= skin friction coefficient based incoming freestream conditions
M_∞	= incoming freestream Mach number
N	= number of fringes
p_o	= stagnation pressure of incoming stream, MPa (psia)
p_w	= wall static pressure on flat plate, MPa (psia)
p_∞	= incoming freestream static pressure, MPa (psia)
R	= radial distance measured from the fin leading-edge, cm (in.)
Re_θ	= Reynolds number based on the local, undisturbed boundary-layer momentum thickness
s	= distance measured along surface streamline, mm
T_{aw}	= adiabatic wall temperature, K
T_w	= wall temperature, K
T_o	= freestream stagnation temperature, K
u^+, y^+	= dimensionless wall-wake velocity and height coordinates
x, y, z	= orthogonal streamwise, normal, and spanwise coordinates, cm
α	= angle made by fin with respect to the incoming freestream direction, deg.
β	= angle with respect to freestream direction, measured from fin leading-edge, deg.
δ	= local, undisturbed boundary-layer thickness, mm
Δs	= distance from oil-film leading edge to laser spot along surface streamline, mm
ν	= oil viscosity, centistokes
Π	= boundary-layer wake-strength parameter
τ_w	= wall shear stress, N/m^2

Introduction

Swept shock wave/boundary-layer interactions are among the chief aerothermodynamic problems which currently limit high-speed propulsion and flight. They also represent a fundamental problem area of modern fluid dynamics which has, thus far, evaded any comprehensive theoretical or computational treatment. Many publications and a recent survey article[1] have appeared on this subject.

The computation of complex viscous-inviscid interacting flows such as the swept shock/boundary-layer interaction is presently paced by the need for detailed, "benchmark" experiments for code validation.[2] In particular, it is widely recognized that traditional measurements such as surface pressure and oil-flow visualization are inadequate for this purpose. The current state-of-the-art Navier-Stokes solvers still employ

* Graduate Research Assistant, Mechanical Engineering Department, Student Member AIAA.

† Associate Professor, Mechanical Engineering Department and Director, Penn State Gas Dynamics Laboratory, Associate Fellow, AIAA.

highly-simplified turbulence models, the efficacy of which is in considerable doubt for complex interacting flows. Experimental data which directly address the turbulent stresses in these flows are sorely needed to advance both the development and validation of turbulence models. Unfortunately, such experiments are extremely difficult and expensive to perform in high-speed flows.

Recognizing this, the participants of the 1980-81 AFOSR-HTTM-Stanford Conference on Complex Turbulent Flows scrutinized the available database and recommended certain directions for future experimentation.[3] Among these was the suggestion that detailed and accurate heat transfer and skin friction data be obtained in high-speed flow experiments. These quantities, being directly linked to turbulent stresses within the boundary-layer, provide a more significant level of comparison with CFD (Computational Fluid Dynamics) results than do, *eg*, surface pressures. Again, however, heat transfer and especially skin friction are difficult to measure with acceptable accuracy in high-speed interacting flows.

The traditional methods for the measurement of skin friction in high-speed flows have been thoroughly reviewed by Winter.[4] Recent developments were also surveyed by Settles.[5] Other than the direct measurement of wall shear stress, τ_w, by a balance, the available techniques infer skin friction from some other measured quantity such as heat transfer or pitot pressure. The validity of such inferential methods is doubtful in complex interacting flows. Further, floating-element balances themselves have serious problems in such flows, especially due to pressure gradients and poor spatial resolution. Thus, for the class of flows in question, reliable measurement techniques have been essentially nonexistent. As a result, there are no known skin friction data in shock/boundary layer interactions of accepatable accuracy for code validation purposes.

A recent development, the Laser Interferometer Skin Friction (LISF) meter, promises to resolve this problem. The LISF meter was invented by Tanner and Blows,[6] and was subsequently refined by Tanner,[7] Monson and Higuchi,[8] Monson, Driver and Szodruch,[9] Monson,[10,11] Westphal, Bachalo, and Houser,[12] and Kim and Settles.[13] It interferometrically senses the time rate of thinning of an oil film on a polished surface subjected to aerodynamic shear. In two-dimensional (2-D) flows without pressure gradients, oil lubrication theory then gives τ_w directly without any reference to the properties of the overlying boundary layer. While some corrections are required in pressure-gradient and shear-gradient flows, the instrument nonetheless delivers essentially a direct measurement of τ_w. The Penn State version of this instrument and its associated data acquisition and reduction procedures[13] is believed to be the only compressible-flow LISF meter currently in existence.

The applicability, repeatability, and accuracy of the LISF technique for use in compressible flows have been determined by Kim and Settles[13] through an experimental calibration over a range of Mach numbers. It was observed that surface-wave phenomena on the oil film limit the technique in high-τ_w flows, but this does not preclude accurate measurements in the supersonic Mach number range. Monson[10] reached a maximum level of $\tau_w = 120$ N/m^2 with the LISF meter in high-Reynolds number supersonic flow. Here, we extend that limit to almost 600 N/m^2.

The present paper reports an experimental study in which the LISF meter is used to measure τ_w distributions in two interactions of fin-generated, swept shock waves with turbulent boundary-layers. The basic research configuration is an unswept, sharp-leading-edge fin of variable angle, α, mounted on a flat plate. This configuration generates "building-block" interactions representative of those occurring on practical high-speed vehicles. Two examples are fin-fuselage junctions and corner flows in supersonic engine inlets.

The goal of this study is to apply the LISF meter to obtain *reliable* τ_w data in three-dimensional (3-D) swept shock wave/turbulent boundary-layer interactions. Such data are sought in order to shed light on the physical mechanisms of such interactions, and to provide a benchmark for CFD code validation. In particular, the data are expected to be useful in judging the effectiveness of current turbulence models.

Experimental Methods

Wind Tunnel and Test Conditions

The Penn State Supersonic Wind Tunnel,[14] used in this study, is a blowdown facility with a nominal Mach number range of 1.5 to 4. The variable Mach number capability is achieved by way of an asymmetric sliding-block nozzle. The test section of the wind tunnel is 150 mm (6 in.) wide, 165 mm (6.5 in.) high, and 610 mm (24 in.) long. Calibration experiments have revealed good flow quality across the available Mach number range. Wind tunnel run durations for the present study ranged from 20 to 30 seconds.

The test Mach number was fixed at 3.03 ± 0.017 in this study. The stagnation conditions of the flow were $p_o = 0.827$ MPa (120 psia) $\pm 1.9\%$ and $T_o = 293.5$ K $\pm 1.4\%$, yielding a freestream unit Reynolds number of 6.19×10^7/m $\pm 2\%$.

The interaction test surface was a flat plate, 500 mm (19.5 in.) long, which spanned the test section. The plate was fitted with both surface-pressure taps and surface thermocouples. An unswept fin shock-generator was positioned with its sharp leading-edge 216 mm (8.5 in.) from the plate leading edge and

26.2 mm (1.03 in.) from the tunnel sidewall. The fin was 100 mm (4 in.) high, 127 mm (5 in.) long and 6.35 mm (0.25 in.) thick. The fin height of about 30δ ensured that the interaction was a semi-infinite one.[1] A sketch of the fin/plate test configuration is shown in Figure 1.

The fin angle-of-attack was varied by a pneumatic fin-injection mechanism mounted through the tunnel sidewall. The bottom of the fin had a rubber seal which ensured that no leakage under the fin occurred during the experiments. Two fin angle-of-attack values, $\alpha = 10°$ and 16°, were tested. The fin angles were determined to 0.1° accuracy using a machinist's protractor.

The flat plate contained 96 surface-pressure taps arranged in concentric circular arcs about the fin leading-edge position. This arrangement was chosen to take advantage of the quasiconical interaction symmetry which has been fully described elsewhere.[1] The pressure-tap arc radii were multiples of 25.4 mm (1 in.). LISF measurements were also made along circular arcs centered about the fin leading-edge. However, these were chosen midway between the pressure-tap arcs in order to avoid interference. For the $\alpha = 10°$ case, the arc radius R for LISF measurements was 114.3 mm (4.5 in.). R was reduced to 88.9 mm (3.5 in.) for $\alpha = 16°$ in order to keep the measurement area away from possible interference due to the fin shock-wave interaction with the wind tunnel sidewall boundary-layer. Finally, some additional LISF data were taken along radii from the conical-flow virtual origin. These radii lay at $\beta = 24°$ for the $\alpha = 10°$ case and $\beta = 38°$ for the $\alpha = 16°$ case.

The undisturbed flat-plate boundary-layer has been surveyed and documented[1-4] for test conditions close to those of the present study (same M_∞, but Re_θ 11% lower than present). Pitot-pressure surveys along the flat-plate centerline and 38 mm (1.5 in.) to each side showed that the test boundary-layer is two-dimensional, turbulent, and in equilibrium in the sense that it satisfies the combined law-of-the-wall/law-of-the-wake with constant Π within the accepted equilibrium range. The test boundary-layer is also near-adiabatic ($T_w/T_{aw} = 1.06 \pm 1.1\%$). The mean velocity profile of the undisturbed boundary-layer at $x = 28$ cm (11 in.) from the flat plate leading edge is shown in Figure 2, along with the corresponding Sun-Childs[15] compressible wall-wake curvefit. The boundary-layer parameters extracted from this curvefit are: $\delta = 4.4$ mm, $Re_\theta = 13408$, $\Pi = 0.63$, and $c_f = 0.0015$. For the higher $Re_\theta = 14915$ of the present study, c_f in the incoming boundary-layer is predicted to be 0.0014 by the Van Driest II theory.

The LISF Meter in High-Speed 3-D Flow

The underlying theory of the LISF technique and examples of its application, mainly in incompressible flows, are thoroughly documented in References 6-12. The adaptation of the LISF meter for use in compressible flows has further been discussed in detail by Kim and Settles.[13] The major limitation of the technique is due to surface-wave phenomena on the oil film in high-τ_w flows, about which more will be said below.

Other than in a supersonic delta-wing demonstration experiment by Monson, et al,[9] the LISF meter has not been used in compressible 3-D flows prior to the present study. One of our goals is to firmly establish the applicability of the instrument to such flows.

It is generally necessary in 3-D LISF measurements to know the direction of the τ_w vector a *priori*, since an accurate knowledge of the distance, Δs, from the oil-film leading edge to laser-beam measuring spot is required. Alternatively, when the dual-beam LISF adaptation is used,[8-12] Δs need not be measured. However, in that case, either the dual beam spots must still be aligned with the local τ_w direction, or else two components of τ_w must be measured with considerable extra effort.

Local τ_w directions may be determined directly from surface-flow visualization results, assuming that these are obtained in a quantitative manner. The kerosene-lampblack-adhesive tape technique[16] is particularly suitable for this, in that it yields undistorted full-scale surface-streak patterns. Angular measurements of local τ_w directions are possible with $\pm 0.5°$ routine accuracy. Such patterns were obtained for the $\alpha = 10°$ and 16° test cases of the present study, and are displayed in Figure 3.

During LISF tests, full-scale transparent overlays of these surface-flow patterns were used to identify the surface-flow direction corresponding to a given position of the laser-beam measuring spot. After applying the oil film to the flat plate, an optical cathetometer (least count: 0.025 mm) aligned normal to the surface-flow direction was used to measure Δs with a repeatability of $\pm 0.6\%$. The leading edge of the oil film was highlighted for this purpose by reflected light from a spotlight positioned outside the wind tunnel. Still, uncertainty of the exact oil-film leading-edge position was the major contributor to uncertainty in Δs. With practice, Δs was measured with an overall accuracy of $\pm 2\%$.

With this technique to obtain accurate Δs measurements along the local surface-flow direction, we were able to use the single-beam LISF meter arrangement shown in Figure 1. The dual-beam method, originally developed from the single-beam method by Monson and colleagues, was, at the time, a solution to the problem of inaccuracy in measuring Δs. However, for 3-D flows the dual-beam approach appears to us to involve added complexity and mechanical alignment difficulties which far outweigh its advantages. With the simpler single-beam method, there is no basic difference in the LISF technique for 2-D and 3-D flows.

Arrangement of LISF Meter and Data Acquisition System

Figure 1 illustrates the components of the single-beam LISF meter used in this study. The beam from a 5-milliwatt linearly-polarized helium-neon laser (1) first passes through a 50% neutral-density filter (2) and an iris diaphragm (3). The beam is then directed downward by a folding mirror (4), and focused by a lens (5), passing through the plexiglas ceiling window (6) of the wind tunnel to form a spot of about 450 μm diameter at an appropriate point (7) on the flat plate. During experiments, a thin film of $\nu = 500$ centistokes Dow-Corning "200" silicone oil applied to a local region (7) of the flat plate is sheared by the τ_w distribution of the shock/boundary-layer interaction due to the fin (8). The incident laser beam is reflected by both the surface of the oil film and the polished plate beneath it. This produces a reflected, two-component, interfering laser beam directed out of the wind tunnel through the ceiling window. (The beam angles of incidence and reflection are kept to about 1°.) The reflected beam is intercepted by two first-surface aiming mirrors, (9) and (10), whence it is directed through a 6328Å filter (11) onto a photodiode (12).

The photodiode senses a time-dependent light intensity due to the interference of light reflected from the oil film and test surface. The photodiode output (13) is raised to a level of 8 volts by an internal operational amplifier, low-pass filtered with a 10 Hz cutoff to remove high-frequency noise, and recorded. Seven other channels of data are recorded simultaneously: p_o, T_o, two p_w channels, and three T_w channels. The 8 data channels are simultaneously sampled by a multiplexer, digitized by a microcomputer-controlled A/D converter, and stored in the computer memory. For present purposes a 20Hz data rate was initially chosen, yielding at least 20 points per interference fringe. However, the requirement for greater accuracy in high-shear regions of the flow led to an increase of the data rate to 50Hz. The photodiode output was also monitored on a stripchart recorder during the experiments.

Data Reduction

A detailed account of LISF data reduction procedures is given by Kim and Settles.[13] Briefly, the limited fringe count obtainable in high-τ_w flows calls for somewhat different data reduction than that reported by other investigators for incompressible flows. Given only 2-8 fringes, it becomes necessary to determine τ_w based on the entire signal within the usable fringe record. Merely determining the time interval corresponding to 3 arbitrary fringe peaks, as is done in incompressible flow, does not yield sufficient accuracy here.

Thus, as described in Reference 13, it is necessary to define that part of the fringe record which is usable and consistent with oil lubrication theory, *ie*, which conforms to a regular "envelope." The initial and final segments of the fringe record which do not so conform are discarded, as are occasional distorted fringe records due to dust particles on the oil film, etc. Usable fringe records are smoothed by repeated application of an adjacent-point averaging algorithm until all noise on the signal is removed.

The LISF data reduction equation,[8] derived from the Navier-Stokes equation and assuming constant wall shear stress, is:

$$\tau_w = \frac{2n\rho\nu cos(r)}{\lambda}\left[\frac{\Delta s}{N't'}\right] \tag{1}$$

where N' = effective fringe number, t' = effective oil flow time, n = oil refractive index, ρ = oil density, λ = laser wavelength, and r = oil refraction angle. For present purposes this equation requires a correction for the effect of variable T_w on ν, as described in Reference 13. The calculation of N' and t' is also carried out per Reference 13, eqns. (6) and (7).

These results are next compared with oil lubrication theory in the N'-t' plane, as shown in Figure 4 for a case where $\tau_w = 586$ N/m^2. A least-squares curvefit of the data to the lubrication theory is performed, followed by a computation of the reduced χ^2 deviation of the data from the fitted curve. Then, the first fringe peak (*ie*, the first data point) is eliminated and the fit is repeated. This process is continued up to $\Delta N = -1.5$, rather than -2 as quoted in Reference 13, considering the small number of usable fringes in the present study (due to high τ_w) compared to our previous work. The value of $N't'$ corresponding to the curvefit with the minimum reduced χ^2 is used in the calculation of τ_w in Equation 1.

Before τ_w is found, however, two further corrections[8,9] are required in principle, since the oil film in the present experiments is subject to both pressure- and shear-gradients. The pressure-gradient correction, per Monson and Higuchi[8], was evaluated through interpolation of p_w measured at the radial tap rows on either side of the LISF measurement arc on the flat plate. These pressure distributions, obtained in an earlier study[14], are plotted in Figure 5 as functions of the angle β. Note that it was deliberately chosen to take LISF data in the region of quasiconical interaction symmetry well downstream of the fin leading-edge. Thus, as shown in Figure 5, p_w vs. β is essentially independent of R. The pressure-gradient correction for the present experiments amounted at most to $\pm 0.1\%$, which is negligible. This fact is significant in that pressure-gradient errors are controlling factors in most other methods of skin friction measurement.[4,5]

Per Monson, Driver, and Szodruch,[9] the shear-gradient correction is quite simple for the single-beam LISF technique. The correction is required if there is a significant change in τ_w from the oil-film leading-edge to the laser-beam measurement spot. This correction has the form:

$$\tau_w' = \tau_w + \frac{1}{4}\frac{\partial \tau_w}{\partial s}\Delta s \qquad (2)$$

where τ_w' = the corrected value of wall shear stress. For small Δs one may assume that $\partial \tau_w / \partial s$ = a constant locally. Thus the correction is accomplished by a shift of the measurement point along the surface streamline direction. However, for the present experiments $\Delta s \simeq 2$ mm, so the required shift is only $\simeq 0.5$ mm, which is negligible. In general, a shear-gradient correction may always be avoided in single-beam LISF measurements if Δs is kept small.

Error Analysis

The uncertainties in the flow quantities and other parameters connected with the LISF measurements have been cited in previous sections. In all cases these uncertainties are given as the mean value $\pm$ one standard deviation. Each measurement point within the two swept interactions studied here was repeated 7 times in separate wind tunnel runs. Chauvenet's criterion was then applied once to each 7-point ensemble to discard, if necessary, a single bad point from the ensemble. The error bars in the plots of the following sections indicate the repeatability of the data as $\pm$ 1 standard deviation about the mean. In general, this repeatability error varied from as little as $\pm 2\%$ upstream of the interaction to as much as $\pm 10\%$ at the highest τ_w in the $\alpha = 10°$ case. In the subsequent $\alpha = 16°$ experiments, a higher data acquisition rate and experience combined to limit the repeatability band to $\pm 6\%$ or less.

Of course, there exists no calibration standard with which to judge the absolute accuracy of τ_w measurements in shock/boundary-layer interactions. However, the accuracy of LISF measurements in compressible flat-plate turbulent boundary-layers has been assessed in previous calibration experiments.[9,13] By coming to terms with the limits imposed by high shear levels on the usable fringe count, the error band has been reduced from $\pm 10\%$[9] to $\pm 6\%$[13] at the Mach number of the present study. As discussed below, further improvements may be possible.

Results and Discussion

The measured skin friction distribution for $\alpha = 10°$, $R = 114.3$ mm (4.5 in.) is shown in Figure 6. As in Figure 5, the c_f data are plotted vs. the angle β measured from the fin leading edge, since the interaction is quasiconical. The flat-plate c_f level ahead of the interaction is 0.0011, which is 20% below the value predicted by the Van Driest II theory. At the upstream-influence line of the interaction ($\beta = 39°$), c_f initially rises, then falls again in the region between the separation line ($\beta = 32°$) and the angle of the "inviscid" fin shock wave ($\beta = 27.4°$). From this location aft to $\beta = 15°$ a steep rise in c_f occurs, reaching maximum values of 0.0025 or 230% of the incoming level. Finally, c_f decreases slightly as the fin ($\alpha = \beta = 10°$) is approached.

Our physical interpretation of the measurements shown in Figure 6 is as follows. The initial rise of c_f at the upstream influence line appears to be due to the onset of the swept pressure gradient, which shears the bottom of the incoming boundary-layer in the spanwise direction. Low-momentum fluid is thus removed from the boundary-layer, such that the velocity-gradient normal to the surface (and thus c_f) is increased. The onset of the swept interaction may therefore be imagined as a natural boundary-layer control mechanism. However, separation nonetheless occurs downstream, where the convergence of upstream and downstream fluid at the wall reduces the normal velocity-gradient and c_f. The steep rise to maximum c_f values near the fin is explained in terms of recent structural studies of separated fin interaction flowfields.[17] The observed "λ-shock" structure causes the impingement of a supersonic jet on the flat plate between the fin and the line of flow reattachment upstream of the fin. This phenomenon is known to produce very high τ_w, p_w, and heat transfer levels.[18] From this jet impingement region the fluid near the wall moves spanwise and forward to eventually meet the separation line. Thus the phenomenology of the region $15° \leq \beta \leq 32°$ in Figure 7 is a rapid *decrease* of c_f from its maximum level as the separation line is approached from behind.

The measured skin friction distribution for $\alpha = 16°$, $R = 88.9$ mm (3.5 in.) is shown in Figure 7. This stronger interaction exhibits the same qualitative c_f features as the 10° case. However, the maximum c_f level is now 0.0041, or 370% higher than the incoming boundary-layer c_f. As the interaction strength grows, the jet-impingement phenomenon described above also grows stronger and produces higher local wall shear, here centered about $\beta \simeq 24°$. The skin friction drops rapidly and almost symmetrically on either side of this impingement region.

The initial rise in c_f at the upstream-influence line, prominent in Figure 6, is almost unnoticeable in Figure 7. Here the upstream influence line lies at $\beta = 49°$ and the separation line occurs at $\beta = 45°$, *ie*, very close together. Previous studies[1,19] have shown that the angular increment between upstream influence and separation decreases with increasing interaction strength, eventually becoming quite small. Thus the initial rise in c_f at the interaction onset is judged to be primarily a weak-interaction phenomenon.

Between the inviscid shock location ($\beta = 33.3°$) and the separation line, c_f decays less rapidly than in its steep fall from the jet-impingement location at $\beta \simeq 24°$. Within this region at $\beta = 37°$ lies a surface-flow feature commonly referred to as "secondary separation," which is quite weak in the present case (see Figure 3b). No indication of its presence is noticeable in the c_f distribution.

Throughout these experiments the performance of the LISF meter was quite consistent with previous experience in simpler flows.[13] The primary noticeable difference in performance was due to high interaction shear levels which preduced fewer usable fringes than before. However, for laser-beam spot locations directly beneath the inviscid fin shock, noisy fringe signals were obtained. This is thought to result from laser-beam refraction by the shock when the two are essentially coplanar. Even so, it was possible to filter out the noise and still obtain a c_f measurement beneath the shock.

Comparison with Navier-Stokes Computations

Computational simulations have been carried out by Horstman and Knight[20] for swept, fin-generated interactions with essentially the same boundary conditions as in the present experiments. These investigators provided the detailed results of their computations[21,22] for comparison with our measured c_f distributions. In all cases the compressible, Reynolds-averaged Navier-Stokes equations were solved, though different numerical algorithms, grids, and turbulence models were used. Horstman's solutions employed the Jones-Launder, 2-equation k-ϵ turbulence model, while Knight used the Baldwin-Lomax algebraic eddy-viscosity turbulence model. A more detailed description of these computations is not given here due to space limitations, but is thoroughly documented elsewhere (*eg*, Reference 20).

A comparison of the Horstman and Knight CFD results with the present $\alpha = 10°$ c_f data is shown in Figure 6. (Note that an interpolation of the computed mesh points of both computations was done by the present authors in order to present all results at $R = 114.3$ mm (4.5 in.) from the fin leading-edge.) Overall, both computations reasonably predict the high measured c_f level around $\beta = 15°$, as well as its decay with increasing β. However, the initial region of the interaction, from the upstream influence to the inviscid shock, is not well predicted in either case. Knight's result shows an initial decrease in c_f, whereas an increase was measured. Horstman's solution does predict the increase, but places it some 5° aft of its measured location. Horstman[21] recognizes that his computational simulations of such interactions tend to underpredict the upstream influence for reasons unknown at present. Knight's solution, on the other hand, matches the experimental upstream influence angle but shows the opposite trend in c_f. The discrepancies in the incoming boundary-layer c_f level in Figure 6 are due, at least in part, to somewhat different Re_θ boundary conditions among the 3 cases compared.

A comparison of the Horstman's CFD result with the present $\alpha = 16°$ c_f data is shown in Figure 7. (No computation for this fin angle was carried out by Knight.) Again, the upstream influence is underpredicted and the initial c_f rise is overpredicted, compared with the measurements. However, Horstman's solution is in good agreement with our results aft of the inviscid shock location at $\beta = 33.3°$.

Finally, the additional LISF data taken along radii from the quasiconical virtual origin at $\beta = 24°$ for the $\alpha = 10°$ case and $\beta = 38°$ for the $\alpha = 16°$ case are shown in Figures 8a and 8b, respectively. In Figure 8a, interpolated values of both the Horstman and Knight computations are also shown. The abscissa of Figures 8a and 8b is given as the streamwise distance from the virtual conical origin of the interaction.[1] This was determined from surface-streak patterns in the experiment and from the computational analogs of such patterns. Presenting the results in these coordinates reveals the behavior of c_f in the inception zone of the interaction and in the quasiconical region downstream.

Figure 8a reveals that c_f increases with distance from the virtual origin, eventually asymptoting to a constant level. The measurements and both computations agree on this point, which is entirely consistent with the quasiconical interaction model proposed earlier.[1] Figure 8b shows the same phenomenon in the $\alpha = 16°$ interaction. Horstman's computation is not shown here because its underprediction of the upstream influence confuses the comparison at the chosen conical ray.

Implications for LISF Measurements in High-Shear Flows

As described elsewhere,[9,13,23] surface-waves on the oil film impose the most serious limitation on the LISF technique. By disrupting the laser-beam coherence, these waves prevent usable interference fringes from being obtained until the oil film becomes quite thin. This effectively limits the number of usable fringes

one can obtain, which directly affects the measurement accuracy. The surface-wave problem is exacerbated as τ_w becomes large.

In the present study we have encountered τ_w levels ranging from 115 to 586 N/m^2. The number of usable fringes we obtained over this range is plotted against τ_w in Figure 9. This Figure indicates that an asymptotic condition of roughly 2 usable fringes may persist even at extremely high shear levels. Actually, the curvefit to the data shown in Figure 9 yields the expression:

$$N = \frac{1500}{\tau_w} - \frac{58370}{\tau_w^2} \tag{3}$$

but extrapolation of this fit to higher τ_w values is not warranted.

The upshot of Figure 9 is the following: If sufficient accuracy in c_f can be had from only 2 interference fringes, then the LISF technique can still be used despite arbitrarily high shear levels. For this reason we have concentrated our efforts here and in Reference 13 on extracting the maximum useful information from an extremely limited fringe count. There appears to be no simple way to increase N, although switching to a green helium-neon laser ($\lambda = 5230$Å) would produce a slight advantage. The fringe count could be at least doubled by the use of a UV-laser, but this approach involves several serious drawbacks.

Conclusions

Experimental measurements have been made of wall shear stresses in swept interactions of a planar shock wave generated by a fin at angle of attack, and the two-dimensional turbulent boundary layer on a flat plate at Mach 3.03. These measurements were made using the Laser Interferometer Skin Friction (LISF) meter. The significant conclusions of this study are as follows:

1. The LISF technique is shown to be practical for skin friction measurements in 3-D shock wave/boundary-layer interactions.
2. With proper data acquisition and reduction procedures, the LISF technique is useful even at extremely-high wall shear stress levels.
3. In contrast with the case for other skin friction methods, the LISF corrections for pressure- and shear-gradients are negligible in the present experiment.
4. Skin friction is found to rise at the onset of a weak swept interaction, and to reach high levels near the fin for both weak and strong interactions.
5. The present skin friction data, obtained in 7-point ensembles at each measuring station, has an overall repeatability of $\pm 6\%$ or better.
6. The quasiconical interaction model proposed earlier is supported by the present results, and
7. Navier-Stokes computations by two other investigators simulate some features of the measured c_f distributions, but fail to predict other features properly.

Acknowledgments

This research was supported by AFOSR Grant 86-0082 from the U. S. Air Force Office of Scientific Research, monitored by Dr. J. D. Wilson. The cooperation of Dr. C. C. Horstman and Prof. D. D. Knight in making available their computational results is greatly appreciated. The use of data from previous experiments by F. K. Lu is gratefully acknowledged. The initial development of the Penn State LISF meter was supported by NASA-Lewis Research Center Grant NAG 3-527, monitored by W. R. Hingst.

References

1. Settles, G. S. and Dolling, D. S., "Swept Shock Wave/Boundary-Layer Interactions," in *AIAA Progress in Astronautics and Aeronautics: Tactical Missile Aerodynamics*, edited by M. Hemsch and J. Nielsen, Vol. 104, AIAA, New York, 1986, pp. 297-379.
2. "Computational Fluid Dynamics Validation," Report of the Ad Hoc Committee on CFD Validation, Aeronautics Advisory Committee, NASA, May 1, 1987.
3. Bradshaw, P. , Cantwell, B. J., Ferziger, J. H., Kline, S. J., Rubesin, M. , and Horstman, C. C., "Experimental Data Needs for Computational Fluid Dynamics--A Position Paper," *Proceedings of the 1980-81-AFOSR-HTTM-Stanford Conference on Complex Turbulent Flows*, eds. S. J. Kline, B. J. Cantwell, and G. M. Lilley, Vol. I, 1981, pp. 23-35.

4. Winter, K. G., "An Outline of the Techniques Available for the Measurement of Skin Friction in Turbulent Boundary Layers," *Progress in the Aerospace Sciences*, Vol. 18, 1977, pp. 1-57.

5. Settles, G. S., "Recent Skin Friction Techniques for Compressible Flows," AIAA Paper 86-1099, May 1986.

6. Tanner, L. H., and Blows, L. G., "A Study of the Motion of Oil Films on Surfaces in Air Flow, with Application to the Measurement of Skin Friction," *Journal of Physics E:Scientific Instruments*, Vol. 9, March 1976, pp. 194-202.

7. Tanner, L. H., "The Application of Fizeau Interferometry of Oil Films to the Study of Surface Flow Phenomena," *Optics and Lasers in Engineering*, Vol. 2, 1981, pp. 105-118.

8. Monson, D. J., and Higuchi, H., "Skin Friction Measurements by a Dual-Laser-Beam Interferometer Technique," *AIAA Journal*, Vol. 19, June 1981, pp. 739-744.

9. Monson, D. J., Driver, D. M., and Szodruch, J., "Application of a Laser Interferometer Skin-Friction Meter in Complex Flows," *Proceedings of the International Congress on Instrumentation in Aerospace Simulation Facilities*, Sept. 1981, pp. 232-243 (IEEE Publication 81CH1712-9).

10. Monson, D. J., "A Nonintrusive Laser Interferometer Method for Measurement of Skin Friction," *Experiments in Fluids*, Vol. 1, 1983, pp. 15-22.

11. Monson, D. J., "A Laser Interferometer for Measuring Skin Friction in Three-Dimensional Flows," *AIAA Journal*, Vol. 22, April 1984, pp. 557-559.

12. Westphal, R. V., Bachalo, W. D., and Houser, M. H., "Improved Skin Friction Interferometer," NASA TM 88216, March 1986.

13. Kim, K.-S., and Settles, G. S., "Skin Friction Measurements by Laser Interferometry," *A Survey of Measurements and Measurement Techniques in Rapidly Distorted Compressible Turbulent Boundary Layers*, eds. Fernholz, H. H., Smits, A. J., and Dussauge, J. P., Ch. 3, AGARDograph to be published in 1988.

14. Lu, F. K., "Mach Number Effects on Fin-Generated Shock-Wave Boundary-Layer Interactions," Ph.D. Thesis, The Pennsylvania State University, to be published in 1988.

15. Sun, C. C. and Childs, M. E., "A Modified Wall-Wake Velocity Profile for Turbulent Compressible Boundary Layers," *AIAA Journal of Aircraft*, Vol. 10, June 1973, pp. 318-383.

16. Settles, G. S. and Teng, H.-Y., "Flow Visualization Methods for Separated Three-Dimensional Shock Wave/Turbulent Boundary Layer Interactions," *AIAA Journal*, Vol. 21, March 1983, pp. 390-397.

17. Lu, F. K., and Settles, G. S., "Structure of Fin-Shock/Boundary-Layer Interactions by Laser Light-Screen Visualization," AIAA paper to be presented at the First National Fluid Dynamics Congress, Cincinnati, OH, July, 1988.

18. Edney, B. E., "Anomalous Heat Transfer and Pressure Distributions on Blunt Bodies at Hypersonic Speeds in the Presence of an Impinging Shock," FFA Report 115, The Aeronautical Research Institute of Sweden, Stockholm, Sweden, February 1968.

19. Lu, F. K., Settles, G. S. and Horstman, C. C., "Mach Number Effects on Conical Surface Features of Swept Shock Boundary-Layer Interactions," AIAA Paper 87-1365, June 1987.

20. Knight, D. D., Horstman, C. C., Shapey, B. L., and Bogdonoff, S. M., "The Flowfield Structure of the 3-D Shock Wave-Boundary Layer Interaction Generated by a 20 Degree Sharp Fin at Mach 3," AIAA Paper 86-0343, January1986.

21. Horstman, C. C., private communication, October 1987.

22. Knight, D. D., private communication, October 1987.

23. Murphy, J. D., and Westphal, R. V., "The Laser-Interferometer Skin-Friction Meter - A Numerical and Experimental Study," *Proceedings of the Third Symposium on Numerical and Physical Aspects of Aerodynamic Flows*, Long Beach, CA, January 1985, Paper 7-1.

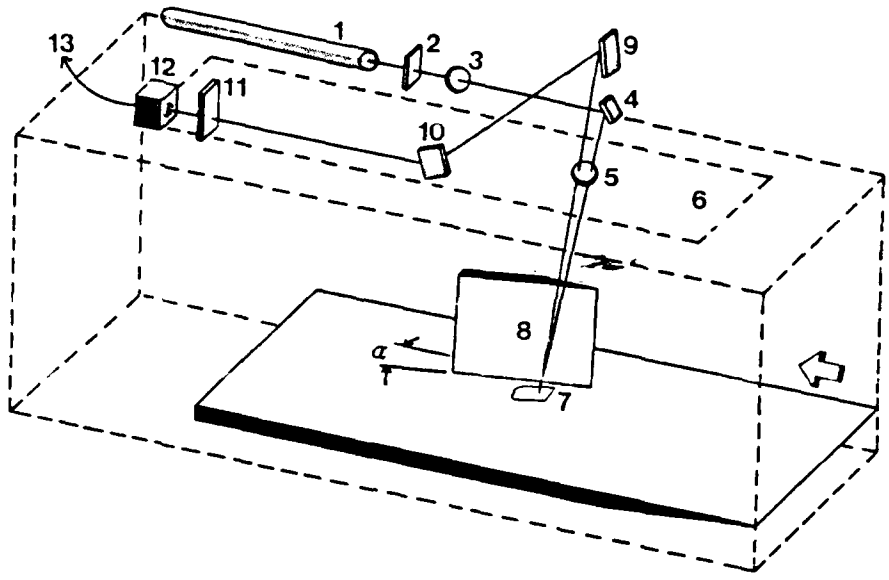

Fig. 1 - Schematic Diagram of LISF Meter, Flat Plate, and Fin (See Text for Key).

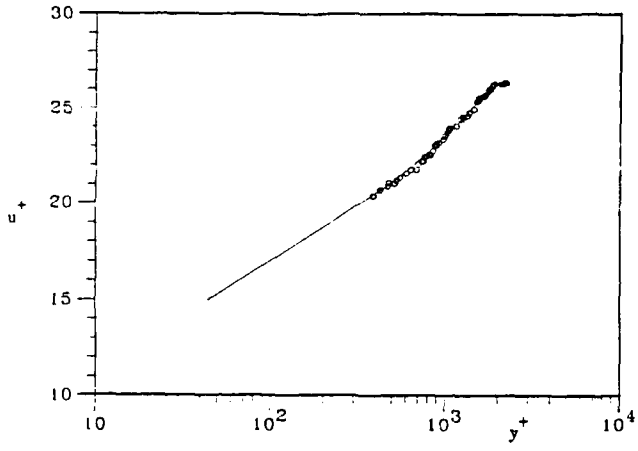

Fig. 2 - Incoming Velocity Profile Wall-Wake Curve-fit.

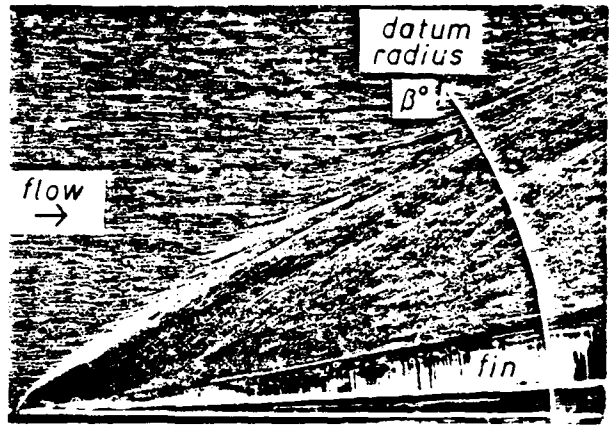

Fig. 3a - Kerosene-Lampblack Surface-Flow Pattern for $\alpha = 10°$.

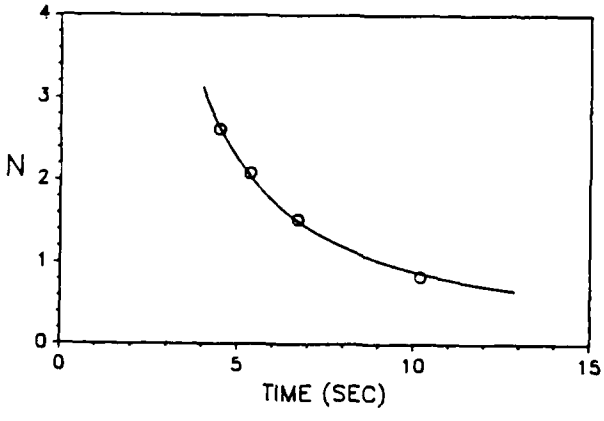

Fig. 4 - Fringe Number vs. Time for $\tau_w = 586$ N/m^2.

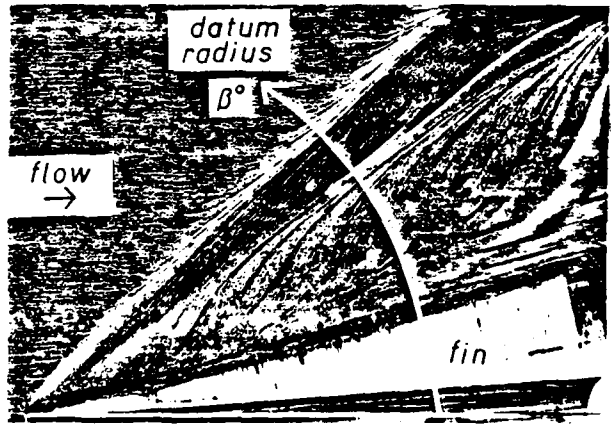

Fig. 3b - Kerosene-Lampblack Surface-Flow Pattern for $\alpha = 16°$.

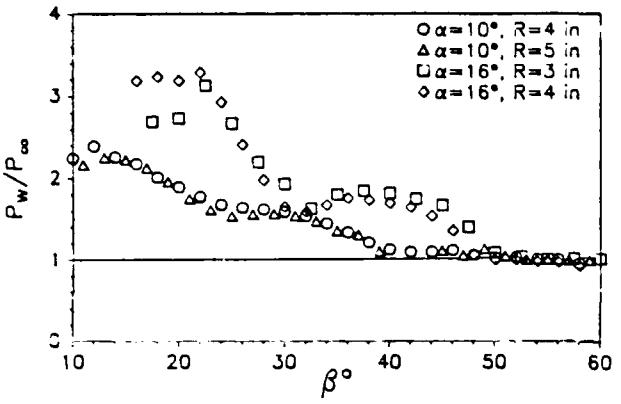

Fig. 5 - Interaction Surface Pressure Distributions for $\alpha = 10°$ and $16°$.

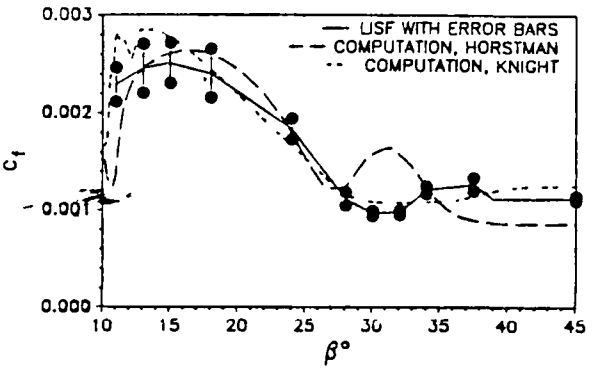

Fig. 6 - c_f Distribution for $\alpha = 10°$ with CFD Comparisons.

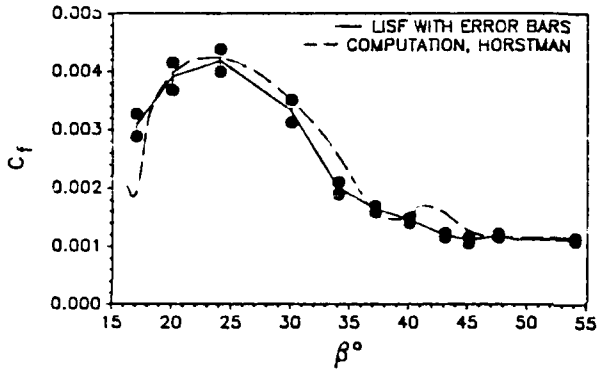

Fig. 7 - c_f Distribution for $\alpha = 16°$ with CFD Comparison.

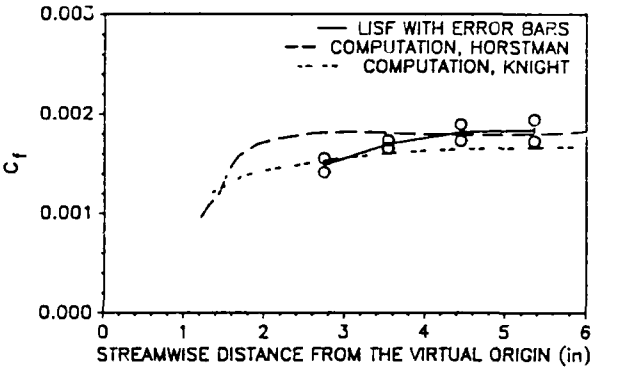

Fig. 8a - c_f Distribution Along $\beta = 24°$ Conical Ray for $\alpha = 10°$.

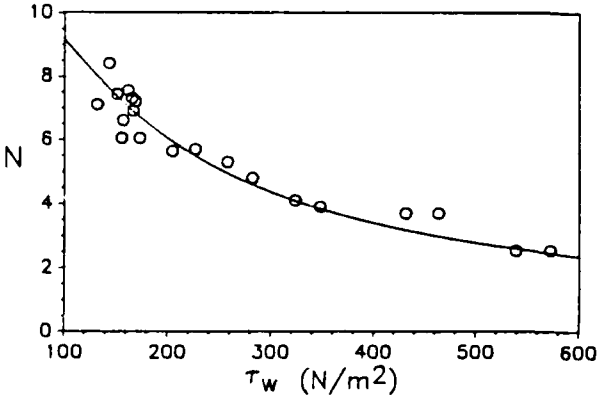

Fig. 9 - Number of Usable Fringes vs. Shear Level.

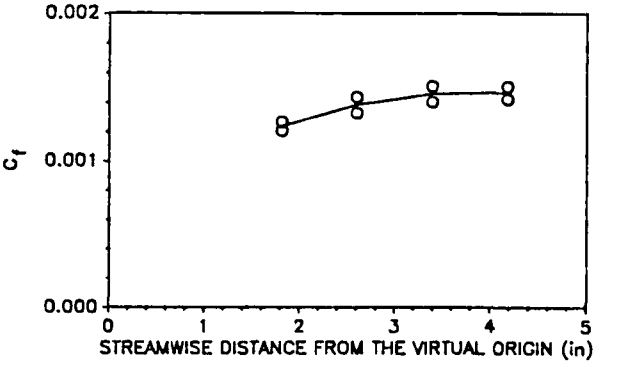

Fig. 8b - c_f Distribution Along $\beta = 38°$ Conical Ray for $\alpha = 16°$.

XII. Appendix C

AIAA Paper 88-2062, Presented at the AIAA 15th Aerodynamic Testing Conference, San Diego, CA, May 18-20, 1988

Microprocessor Control of High-Speed Wind Tunnel Stagnation Pressure

Y-T Fung,* G. S. Settles,† and A. Ray,‡
Pennsylvania State University, University Park, PA, 16802

Abstract

The development and implementation of a control algorithm for the microprocessor-based stagnation pressure control system of the Penn State Supersonic Wind Tunnel Facility is reported. The gas dynamics and the control-valve characteristics of this blowdown-type facility are nonlinearly related. A mathematical model was developed for the open-loop system characteristics and was linearized for the controller design. A single-input, single-output PI controller was chosen for this task because of its simplicity and availability. The resulting performance of the supersonic wind tunnel was found to be quite good, with stagnation pressure variations typically held to within 1 to 2 percent.

Nomenclature

A = test section area, m^3
A_* = nozzle throat area, m^3
C_g = control valve "gas sizing coefficient"
c_v = specific heat at constant volume, J/kg-K
c_p = specific heat at constant pressure, J/kg-K
h_v = specific enthalpy of air through valve, J/kg
h_* = specific enthalpy of air through nozzle, J/kg
K_p = controller proportional gain
K_i = controller integral time
M = test section Mach number
m_t = storage tank air mass, kg
$\dot{m}_v$ = mass flow rate through valve, kg/sec
m_o = stilling chamber air mass, kg
$\dot{m}_*$ = mass flow rate through nozzle throat, kg/sec
P_d = desired stagnation pressure, Pascal
P_t = storage tank air pressure, Pascal
P_o = stagnation pressure, Pascal
R = gas constant, J/kg-K
T_t = storage tank air temperature, K
T_o = stagnation temperature, K
U_t = storage tank air internal energy, Joule
U_o = stilling chamber air internal energy, Joule
V_t = storage tank volume, m^3
V_o = stilling chamber volume, m^3
v_v = velocity of air through valve, m/sec
v_* = velocity of air through nozzle throat, m/sec
Θ = valve opening position, deg
ρ_t = storage tank air density, kg/m^3
ρ_o = stilling chamber air density, kg/m^3

* Graduate Research Assistant, Mechanical Engineering Department

† Associate Professor, Mechanical Engineering Department, Associate Fellow AIAA.

‡ Associate Professor, Mechanical Engineering Department, Member AIAA.

Introduction

This paper deals with the solution of the stagnation pressure control problem in the Penn State Supersonic Wind Tunnel Facility. A sketch of the facility is shown in Fig 1. This facility is a blowdown-type wind tunnel with an asymmetric sliding-block nozzle which yields a variable Mach number capability over the range of Mach 1.5 to 4.0. Dry air is stored in a 56.6 m^3 tank at up to 2.07 MPa. Testing requirements call for regulated stagnation pressures in the range of 0.34 MPa to 1.72 MPa for typical test durations of 15 to 45 seconds.

The wind tunnel air supply system is equipped with a 20.3 cm diameter, pneumatically-actuated ball valve. If this valve is held at a fixed position, the wind tunnel stagnation pressure drops during testing because the pressure in the storage tank is continuously decreasing. Pressure regulation by manually adjusting the valve opening during a test is possible but inaccurate. An obsolete electromechanical pressure controller has been used in the past, but with unsatisfactory performance for current testing requirements.

For example, at a given Mach number, it is sometimes required to maximize the test duration by running the tunnel at the lowest possible stagnation pressure which will maintain supersonic flow. Similarly, it is often necessary to obtain different Reynolds numbers at a given Mach number by way of preset levels of the stagnation pressure. In all cases, a constant stagnation pressure during testing is a basic requirement.

The purpose of the present work is to design and implement a controller which senses the stagnation pressure and adjusts the valve automatically, thus maintaining the stagnation pressure constant regardless of test Mach number.

Control systems for incompressible fluids have been discussed extensively in the literature[1,2]. However, comparatively little study has been made of the control problems of highly-compressible flows. The major difficulty here lies in the nonlinearity of both the gas dynamics and the valve-nozzle characteristics in the case of a supersonic wind tunnel. Furthermore, in this case a wide variety of operating conditions must be handled as described previously. Finally, a highly-sophisticated control system is impractical from considerations of economy and reliability of wind tunnel operations.

A satisfactory solution to this control problem has been achieved through a single-loop *Proportional-plus-Integral* (PI) controller with constant parameter settings. The first step in designing this control system is to develop a mathematical model for the supersonic wind tunnel flow, as described below. An evaluation of various control algorithms is then presented, along with the rationale for the selection

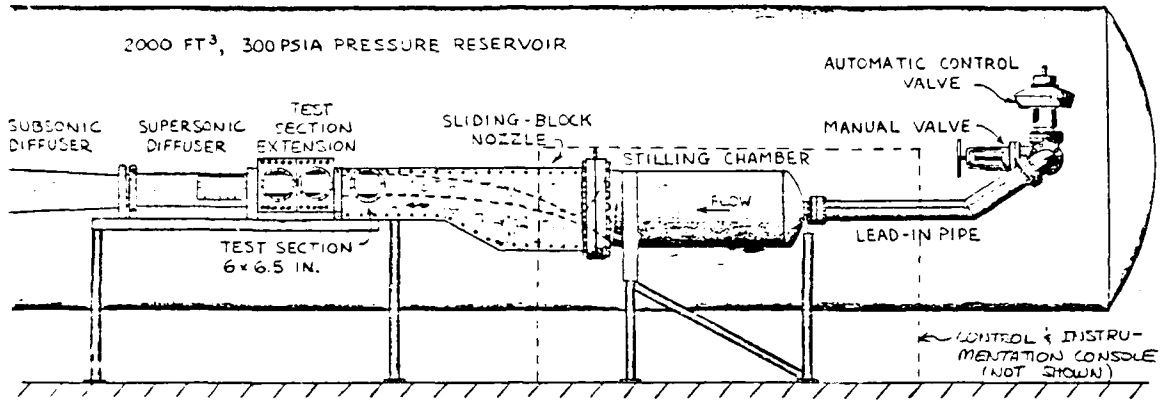

Fig. 1 The Penn State Supersonic Wind Tunnel

of the most suitable one for present purposes. The behavior of the control system has been simulated by computer before its actual implementation. Finally, its performance has been verified by wind tunnel experiments, whose results are compared with the computer simulation.

Mathematical Model

A prerequisite for the control system design is the development of a mathematical model of the controlled process, which is the flow in the supersonic wind tunnel. Two control volumes are selected for this analysis: the air storage tank and the wind tunnel stilling chamber. It is here assumed that all thermodynamic processes are isentropic during a wind tunnel test (no shock waves, frictional losses, or heat transfer), and that the change of potential energy of the gas is negligible. In reality, it is recognized that only the last assumption is strictly correct.

Model Equations for the Storage Tank

Conservation of Mass During a test, it is assumed that the pressure, temperature and density distribution are uniform over the entire control volume. Hence, the rate of decrease of mass in the air tank is equal to the rate of mass efflux through the control valve:

$$V_t \frac{d\rho_t}{dt} = -\dot{m}_v$$

or

$$\frac{d\rho_t}{dt} = -\frac{1}{V_t}\dot{m}_v \tag{1}$$

The valve characteristics are described in literature[3,4] by its manufacturer. The mass flow rate at different valve positions is given by:

$$\dot{m}_v = \frac{2.2958 \times 10^{-8}}{\sqrt{T_t}} C_g P_t \sin\left(2.71\sqrt{\frac{\Delta P}{P_t}}\right)_{\text{rad}} \tag{2}$$

where ΔP is the pressure difference across the valve, here assumed to be given by $\Delta P = P_t - P_o$.

Conservation of Energy By assuming that the energy loss through the control valve is negligibly small, the internal energy change in the air tank is set equal to the enthalpy and kinetic energy flux through the valve,

$$\frac{dU_t}{dt} = -\dot{m}_v h_v - \frac{1}{2}\dot{m}_v v_v^2 \tag{3'}$$

The left-hand side of this equation can be written as:

$$\frac{dU_t}{dt} = \frac{d}{dt}\left[m_t c_v T_t\right] = \frac{d}{dt}\left[\frac{c_v P_t V_t}{R}\right] = \frac{c_v V_t}{R}\frac{dP_t}{dt}$$

Assuming the airflow to behave both calorically and thermally as a perfect gas, the right-hand side becomes:

$$\dot{m}_v h_v + \frac{1}{2}\dot{m}_v v_v^2 = \dot{m}_t h_t = \dot{m}_v c_p T_t$$

Thus, Equation (3') can be written as:

$$\frac{c_v V_t}{R}\frac{dP_t}{dt} = -\dot{m}_v c_p T_t$$

or

$$\frac{dP_t}{dt} = -\left(\frac{c_p R}{c_v V_t}\right)\dot{m}_v T_t \tag{3}$$

Model Equations for the Stilling Chamber

Conservation of Mass Air flows into the stilling chamber from the valve connected to the air storage tank, and flows out through the converging-diverging nozzle to the test section. Therefore, the rate of mass influx into the stilling chamber control volume minus the rate of mass efflux yields the net rate of mass buildup in the stilling chamber,

$$V_o \frac{d\rho_o}{dt} = \dot{m}_v - \dot{m}_*$$

or

$$\frac{d\rho_o}{dt} = \frac{1}{V_o}\left(\dot{m}_v - \dot{m}_*\right) \tag{4}$$

The mass flow rate through the nozzle is a function of stagnation conditions and nozzle throat area[5,6]:

$$\dot{m}_* = \frac{0.6847 P_o A_*}{\sqrt{R T_o}} \tag{5}$$

For a specific test Mach number M and test section area A, the nozzle throat area is given by:

$$A_* = \frac{1.728 A M}{\left(1 + 0.2 M^2\right)^3} \tag{6}$$

Conservation of Energy The energy entering the stilling chamber from the valve with mass $\dot{m}_v$ minus the energy exiting through the nozzle with mass $\dot{m}_*$ is equal to the rate of increase of internal energy in the stilling chamber,

$$\frac{dU_o}{dt} = \dot{m}_v h_v + \frac{1}{2}\dot{m}_v {v_v}^2 - \dot{m}_* h_* - \frac{1}{2}\dot{m}_* {v_*}^2 \qquad (7')$$

The left-hand side can be written as:

$$\frac{dU_o}{dt} = \frac{d}{dt}\left[m_o\, c_v\, T_o\right] = \frac{d}{dt}\left[\frac{c_v\, P_o\, V_o}{R}\right] = \frac{c_v\, V_o}{R}\,\frac{dP_o}{dt}$$

Rewriting the right-hand side of Eqn. (7') in terms of c_p:

$$\dot{m}_v h_v + \frac{1}{2}\dot{m}_v {v_v}^2 = \dot{m}_t\, h_t = \dot{m}_v\, c_p\, T_t$$

$$\dot{m}_* h_* + \frac{1}{2}\dot{m}_* {v_*}^2 = \dot{m}_*\, h_o = \dot{m}_*\, c_p\, T_o$$

Therefore, the statement of energy conservation for the stilling chamber becomes:

$$\frac{c_v\, V_o}{R}\,\frac{dP_o}{dt} = \dot{m}_v\, c_p\, T_t - \dot{m}_*\, c_p\, T_o$$

or

$$\frac{dP_o}{dt} = \left(\frac{c_p\, R}{c_v\, V_o}\right)\left(\dot{m}_v T_t - \dot{m}_* T_o\right) \qquad (7)$$

Mathematical Model for the Wind Tunnel

From the preceding discussion, these expressions were obtained which describe the characteristics of the airflow in the supersonic wind tunnel:

$$\frac{d\rho_t}{dt} = -\frac{1}{V_t}\dot{m}_v \qquad (1)$$

$$\frac{dP_t}{dt} = -\left(\frac{c_p\, R}{c_v\, V_t}\right)\dot{m}_v\, T_t \qquad (3)$$

$$\frac{d\rho_o}{dt} = \frac{1}{V_o}\left(\dot{m}_v - \dot{m}_*\right) \qquad (4)$$

$$\frac{dP_o}{dt} = \left(\frac{c_p\, R}{c_v\, V_o}\right)\left(\dot{m}_v T_t - \dot{m}_* T_o\right) \qquad (7)$$

where the mass flow rate through the valve and the nozzle are given by Eqns. 2, 5 and 6.

Expressing temperature as a function of pressure and density via the perfect-gas equation of state, the above equations become four first-order nonlinear ordinary differential equations in the four state variables P_t, ρ_t, P_o and ρ_o. The inputs to this system are: test Mach number M, which specifies the nozzle geometry, and valve position Θ, which determines the valve behavior. The output of the system is the stagnation pressure P_o. The system of equations was solved for $P_o(M, \Theta)$ by way of a standard finite-difference computer routine.

In order to judge the accuracy of this mathematical model, experimental and simulated results for stagnation pressure vs. time at Mach 4 with the control valve fully open are compared in Fig. 2. The initial air pressure of the storage tank in this comparison is 1.8 MPa (260 psia). The startup process of the wind tunnel involves about a 2-second delay which is not simulated by the model. Otherwise, however, the model accurately predicts the observed rate of decay of P_o with time.

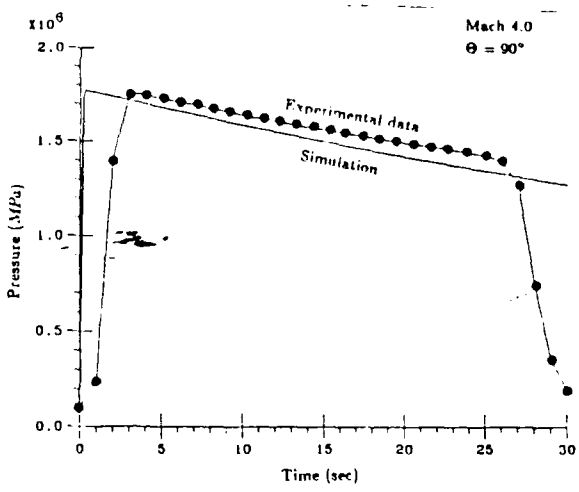

Fig. 2 Stagnation Pressure vs. Time, Valve Fully Open

Controller Design

Control Algorithm Analysis

Upon establishing the mathematical model for the supersonic wind tunnel, a control algorithm based on this model was sought. The goals of the control action of this algorithm are:

(1) To obtain a constant steady-state stagnation pressure with as little transient oscillation as possible,
(2) To maintain this constant pressure as long as possible, and
(3) To meet the above requirements at any desired combination of test Mach number and stagnation pressure within the ranges cited previously.

Several candidate control algorithms were considered for this task, including optimal control, state feedback control and single-loop PID control.

In the optimal control of a process, a control decision is made, subject to certain contraints, that will minimize some measure of deviation from the ideal performance[7]. The performance index of the system evolves from a consideration of such factors as stability, efficiency, economy, reliability, etc. Once the performance index is defined, the best possible system is that which minimizes this index, subject to the contraints imposed upon the system.

In short, the present wind tunnel control problem is relatively simple in that only accuracy and stability are matters of prime concern. It was thus judged that the complexities of optimal control are neither needed nor desired for present purposes.

The state-space control method is based on the description of the system in terms of n first-order differential equations[8]. In the present case, Eqns. 1, 3, 4, and 7 are the state-space equations of the dynamic system, and P_t, P_o, ρ_t and ρ_o are the state variables of this system. The design of a full state feedback controller involves the mathematical description of the desired system response, followed by a determination of the feedback gain of each state variable that yields this response. At present, however, only two state variables, P_t and P_o, are directly measurable. Real-time calculation of ρ_t and ρ_o would thus be required, rendering

this approach cumbersome and potentially expensive to implement. Once again, a simpler approach is called for, *eg*, PID control.

The principle of the PID control scheme is to act upon the variable under control through a proper combination of three control actions: Proportional, Integral, and Derivative control[9]. Proportional control is proportional to the actuating error signal (the difference between the input and the feedback signal) itself, while integral and derivative control are proportional to the integral and derivative of the actuating error signal, respectively. For the present supersonic wind tunnel application of PID control, the input to the controller is the desired stagnation pressure P_d, while the feedback signal is the actual stagnation pressure P_o. This feedback control process is represented by a block diagram shown in Fig. 3.

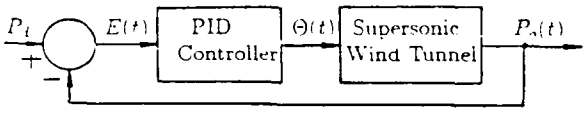

Fig. 3 Block Diagram of PID Control Process

The effects of proportional, integral and derivative control action on the system performance are briefly described as follows: Proportional control is the algorithm in which the change in the control signal is proportional to the deviation of the system output from the desired value[10]. Sole proportional control of a process introduces a steady-state error, or offset, in the response to a step input. This is the chief disadvantage of a purely-proportional controller.

The integral control of a process is equivalent to adding an integrator to an open-loop system[11]. integral control action at any instant is proportional to the area under the actuating error signal curve up to that instant. As long as there is an error signal, the integral controller produces an output to reduce this error. Therefore, the steady-state error of a proportional control system can be eliminated if integral control is added.

Derivative control action responds to the rate of change of the actuating error. It thus "anticipates" the error and initiates an early corrective action. Where required, this tends to increase the transient response and stability of the system.

Overall, PID control is a well-developed method for a single-input single-output system. Only one measurement of a system output is needed for the control process. The simplicity and reliability of PID control are its major advantages over other methods. Moreover, it is usually the least expensive choice of those discussed above. These advantages led to the choice of the PID process for the solution of the present supersonic wind tunnel control problem.

Controller Design Analysis

The transients at startup and shutdown of the supersonic wind tunnel are quite brief. Thus the major concern in controller design is focused on the steady-state performance of the wind tunnel. In order to achieve and maintain a preselected value of stagnation pressure, both proportional and integral control actions are clearly required. However, the transient-handling capability of derivative control is not obviously needed. Thus, for simplicity, we consider only a proportional-plus-integral (PI) controller at present. The possible need for additional derivative control may be judged from the experimental results to be presented later.

The transfer function of a PI controller is given by:

$$G(s) = \frac{\Theta(s)}{E(s)} = K_p \left(1 + \frac{1}{K_i\, s}\right) \tag{8}$$

where s stands for the time-derivative in the Laplace domain and $E(s)$ is the error signal between the reference input P_d (desired stagnation pressure) and the system output P_o (the actual pressure measured in the stilling chamber). The above equation can be rewritten to yield:

$$\Theta(s) = K_p \left(1 + \frac{1}{K_i\, s}\right)\Big(P_d - P_o(s)\Big), \quad \text{or}$$

$$s\,\Theta(s) = K_p\, s \Big(P_d - P_o(s)\Big) + \frac{K_p}{K_i}\Big(P_d - P_o(s)\Big) \tag{9}$$

Applying the inverse Laplace transform in Eqn. 9, the differential relationship between the input $\Xi(t) = P_d - P_o(t)$ and output $\Theta(t)$ of the PI controller is:

$$\frac{d\Theta(t)}{dt} = -K_p \frac{dP_o(t)}{dt} + \frac{K_p}{K_i}\Big(P_d - P_o(t)\Big) \tag{10}$$

where the term $dP_o(t)/dt$ is known from the relation of energy conservation of the stilling chamber (Eqn. 7).

The open-loop system (*ie* without feedback control) is highly nonlinear, both in terms of the gas dynamics and the control valve characteristics. Following standard control-theory procedure, the system was linearized at selected Mach numbers and stagnation pressures over the operating range of the wind tunnel facility. This was done by way of Taylor-series expansions, dropping all higher-order terms.

Next, the controller parameters for different operating points were determined as follows:

(1) A desired closed-loop system with specified pole locations is established first.
(2) The PI control action (Eqn. 10) is added to the linearized model for different operating conditions.
(3) The linearized model together with the control action is fitted to the desired closed-loop system to determine suitable controller parameters K_p and K_i. A proper combination of K_p and K_i relocates the poles of the linearized open-loop system to the desired locations determined in step (1) above.

Values of K_p and K_i were thus found for each desired operating condition. These values were observed to vary by no more than about 20% over the entire wind tunnel Mach number and stagnation pressure range. Thus, as a first approximation, constant average values of $K_p = 0.00014$ and $K_i = 0.08\,\text{sec}^{-1}$ were assumed for all operating conditions. If this approach later proves not to be sufficiently accurate, the controller parameters may be allowed to vary as functions of the wind tunnel operating conditions, using the concept of gain scheduling[9].

Closed-Loop System Mathematical Model

The PI control action (Eqn. 10) together with the original open-loop system mathematical model (Eqns. 1, 3, 4,

and 7) yield a set of expressions for the complete feedback control system. Combining Eqns. 7 and 10, the control action of the PI controller takes the following form:

$$\frac{d\Theta}{dt} = K_p \left(\frac{c_p R}{c_v V_o} \right) (\dot{m}_e T_o - \dot{m}_v T_t) + \frac{K_p}{K_i} (P_d - P_o) \quad (11)$$

Thus the complete mathematical description of the closed-loop system is described concisely by Eqns. 1, 3, 4, and 7, representing the gas dynamics of the supersonic wind tunnel, and Eqn. 11 representing the control action of the PI controller. The desired stagnation pressure P_d in Eqn. 11 is the reference input of this closed-loop system.

Analysis of Closed–Loop System Simulation

As was done for the open-loop wind tunnel equations described previously, the above mathematical model for the closed-loop system has been solved by a finite-difference computer routine. The resulting pressure–time curves for both the storage tank and stilling chamber for test section Mach numbers of 2.5 and 4.0 are shown in Figs. 4a and 4b, respectively. The valve opening position vs. time is also shown for the Mach 2.5 case in Fig. 4c.

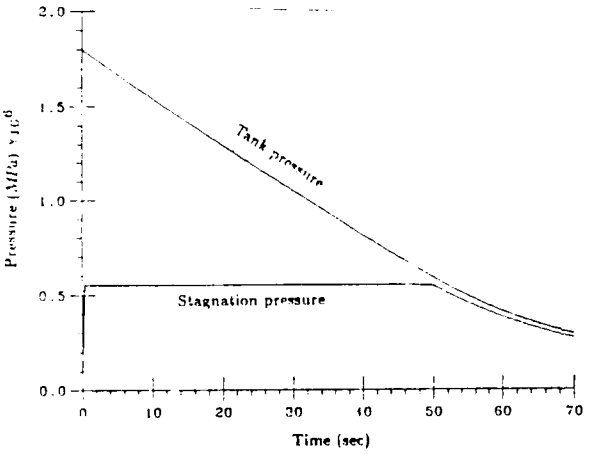

Fig. 4a Controlled P_o vs. Time at Mach 2.5

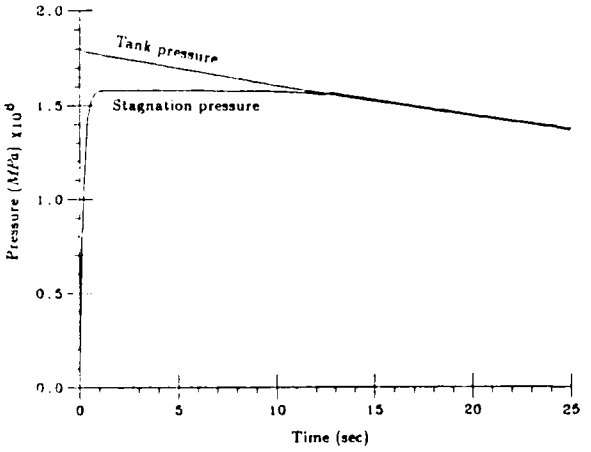

Fig. 4b Controlled P_o vs. Time at Mach 4.0

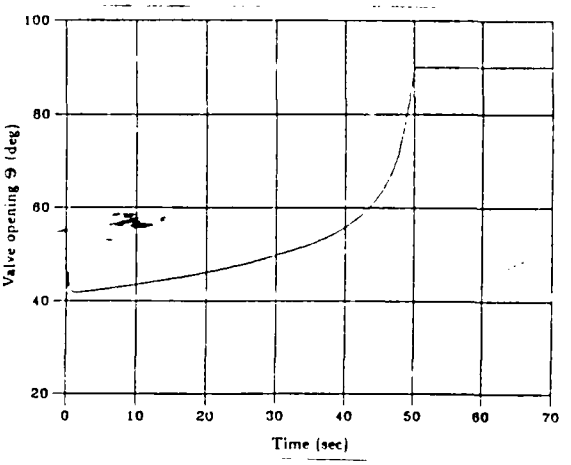

Fig. 4c Valve Opening Position vs. Time at Mach 2.5

Analysis of the simulation results reveals the following:

(1) The constant average controller parameters found above (K_p = 0.00014 and K_i = 0.08 sec^{-1}) are effective at all Mach numbers in obtaining a response with a minimum steady-state error and overshoot as well as a minimum settling time. These controller settings were also found to be capable of maintaining the different steady-state stagnation pressures constant for all Mach numbers in the range of 2.5 to 4.0. Thus the only required input to the closed-loop system is the desired reference pressure P_d.

(2) Maximum-duration testing is possible by presetting P_d to the minimum value to sustain supersonic flow at a given Mach number. Similarly, variable-Reynolds number testing is possible over a wide P_o range at a given Mach number. Of course, the simulation predicts shorter test durations for higher P_o values. However, both these modes of testing are well-simulated using the fixed controller parameters found above.

(3) At a given Mach number and a given reference input, the effects of adjusting the controller parameters on the system response are as follows:

- If the proportional gain is increased, the maximum pressure overshoot and the settling time are increased. But at the same time, the steady-state response can be maintained for a longer time.
- If the proportional gain is decreased, oscillations of P_o during the initial transient period are reduced, but the steady-state test time is also reduced. This is because a higher proportional gain makes the system response more oscillatory, but it also responds more readily to the dropping tank pressure, especially near the end of the test when a large increase in valve opening is called for.
- Changing the integral time within a certain range does not have an obvious influence on the closed-loop system response.

Microprocessor Controller Implementation

Having developed a successful theoretical model for the supersonic wind tunnel and its stagnation pressure controller, we now consider the hardware aspect of the problem. A suitable commercially-available microprocessor PID controller (Moore Products Co. MYCRO-352[10]) was obtained and installed in the console of the Penn State Supersonic Wind Tunnel. While not designed specifically for this application, this controller is programmable with built-in function blocks which may be configured to yield a wide variety of different control algorithms.

The microprocessor controller communicates with the wind tunnel via built-in A/D and D/A converters. The former accepts and digitizes an amplified signal representing the "process variable" from a pressure transducer which senses P_o in the stilling chamber. The latter sends a 4 mA to 20 mA analog output signal to a "reverse" (current-to-pressure) transducer which modulates the air pressure to the bellows-type control valve actuator. Single-input, single-output operation is thus achieved, with all controller actions either taking place automatically within the microprocessor controller or resulting from manual input to the controller by the wind tunnel operator.

Prior to a wind tunnel test, the operator preselects the desired stagnation pressure P_d and enters a corresponding "set point" on the display of the controller. The "set point" and the "process variable" provide inputs to the internal PID controller function block of the MYCRO-352, which compares these to find the actuating error signal, then calculates and produces an appropriate output signal to the control valve.

Other operator inputs to the microprocessor controller include K_p, K_i, and the derivative gain (here set to zero). Manual valve control is also available to the operator by way of an automatic/manual switch. An auxilliary on/off switch in the controller output line is used to initiate and terminate wind tunnel runs. For safety reasons, the control valve actuator is set up such that either a loss of signal from the controller or a loss of electrical power in the laboratory will result in immediate valve closing.

The panel display of the microprocessor controller provides the wind tunnel operator with information including the set point, process variable, and valve opening indices. A bar-graph display allows visual comparison of the actual vs. preselected stagnation pressure levels. Various alarm functions are available for programming if desired. Finally, a pulser knob is provided for manual input to the controller by the operator. Further details on the controller and its programming may be found in Refs. 10 and 11.

Experimental Verification and Discussion

The computer simulation of the wind tunnel and control system has been compared with the actual operation of the Penn State Supersonic Wind Tunnel. In so doing, the simulation served as an important guide in understanding the relationship between control action and the corresponding closed-loop system response, and in allowing the trial-and-error to be done by computer instead of in the actual wind tunnel.

A comparison of the stagnation pressure vs. time of the model simulation and the wind tunnel test data is shown in Figs. 5a-c for Mach 2.5, 3.0, and 3.5. The closed-loop system

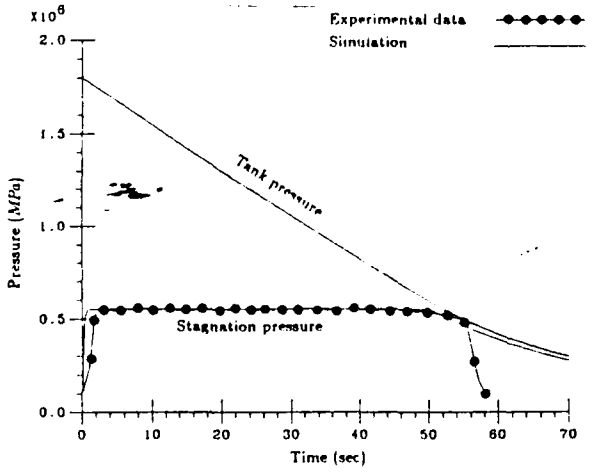

Fig. 5a Comparison of Simulation and Data at Mach 2.5

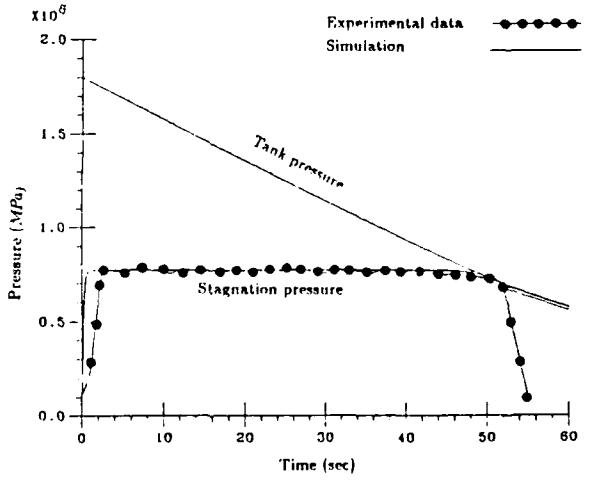

Fig. 5b Comparison of Simulation and Data at Mach 3.0

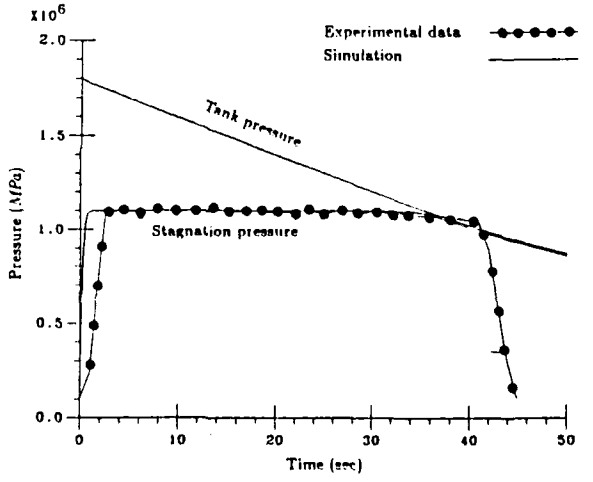

Fig. 5c Comparison of Simulation and Data at Mach 3.5

response of the supersonic wind tunnel is very similar to the results predicted by the model simulation. In every case a constant controlled P_o was obtained in close agreement with the model. The few features of the real feedback control system not predicted by the simulation are discussed below:

(1) The same constant controller parameters determined in the simulation were used in the experiments and were found to be suitable for all Mach numbers in the range of 2.5 to 3.5 at different stagnation pressures. However, Mach numbers below 2.5 were not attempted in the experiments due to tunnel blockage caused by the flat-plate model installation in the test section.

(2) In the final seconds of a run, the valve should open very rapidly to maintain a constant P_o. In reality, however, the valve actuator cannot respond at the required rate for this to occur. This actuator lag is not accounted for in the simulation. Thus, in actual testing, when the tank pressure is only 20–30 *psia* above the steady-state stagnation pressure, both pressures will decrease gradually.

(3) For the test results reported here, no second-throat diffuser was installed in the wind tunnel facility. The minimum running stagnation pressures are thus rather high, ranging from 80 *psia* at Mach 2.5 to 220 *psia* at Mach 4.0. Only quite short runs were possible at Mach 4.0 in this case, since the initial difference between the tank pressure and P_o was at most 60 *psia*. The recent installation of a fixed second throat has increased this difference to 100 *psia* or more, providing a more reasonable Mach 4.0 testing capability of at least 30 seconds at constant P_o. No change in controller programming was required in this case.

(4) The filter breakpoint frequency of the A/D converter in the MYCRO-352 controller is 10 *Hz*. This means that the controller is unaware of any change in the feedback signal between 1/10 sec sample intervals. Since the controller output is a step function, the closed-loop system response is adjusted every 0.1 second, giving a slightly oscillatory driving output to the valve actuator. It is unlikely that the actuator can respond at this frequency. Small oscillations do occur in the measured P_o of the wind tunnel, but these amount at most to only 2 *psia* for $P_o = 160$ *psia* (1.2 %), which is considered acceptable.

Summary

Achieving constant stagnation pressure is a critical concern for supersonic blowdown wind tunnel testing. In the present study, a control algorithm has been developed to achieve this. The control algorithm is designed such that it is suitable for different Mach number testing and, at the same time, obtaining the maximum test time for different stagnation pressures.

A mathematical model based on the thermodynamic properties of air was established for the supersonic wind tunnel. Comparison of the system response of the model simulation and the actual wind tunnel test data was made to determine the applicability of the model. Once a suitable system model was found, it was then used to design the stagnation pressure controller.

After investigating different control algorithms, a single-input, single-output PI controller was chosen for this task because of its simplicity and availability. The major problem in implementing this control system is the high degree of nonlinearity of both the gas dynamics and the control valve characteristics. A linearized mathematical model was used to analyze the open-loop system characteristics as well as for the controller design.

A microprocessor-based PID controller was installed in the Penn State Supersonic Wind Tunnel and programmed according to the computer prediction. The resulting performance of the wind tunnel at different Mach numbers and stagnation pressures was quite good, with the stagnation pressure typically being held constant to within 1% to 2% over a wide range of testing conditions.

Acknowledgement

The microprocessor controller and transducers used in this study were obtained under AFOSR Grant 84-184, a Defense University Research Instrumentation Grant monitored by Drs. M. S. Francis and J. D. Wilson.

References

1. Ogata, K., *System Dynamics.* Englewood Cliffs, N.J., Prentice-Hall, 1978.
2. Palm, W. J., *Modeling, Analysis, and Control of Dynamic Systems.* New York, John Wiley & Sons, 1983.
3. Anon., "Rotary Shaft Control Valve Specifications." Marshalltown, Iowa, Fisher Controls Company, 1984.
4. Anon., "Universal Valve Sizing Rule Instruction Manual." Marshalltown, Iowa, Fisher Controls Company, 1984.
5. White, F. M., *Fluid Mechanics.* New York, McGraw-Hill, 1979.
6. John, J. E. A., *Gas Dynamics.* Newton, Mass., Allyn and Bacon, 1984.
7. Kirk, D. E., *Optimal Control Theory.* Englewood Cliffs, N.J., Prentice-Hall, 1970.
8. Ogata, K., *State Space Analysis of Control Systems.* Englewood Cliffs, N.J., Prentice-Hall, 1967.
9. Shinskey, F. G., *Process Control Systems.* New York, McGraw-Hall, 1979.
10. Anon., "MYCRO-352 Single Loop Digital Controller User's Manual." Spring House, PA, Moore Products Co., 1984.
11. Fung, Y-T., "Microprocessor Control of High-Speed Wind Tunnel Stagnation Pressure," MSE Thesis, Mechanical Engineering Department, Penn State University, Dec. 1987.